NAVAL POSTGRADUATE SCHOOL
Monterey, California

THESIS

DESIGN AND PROTOTYPE DEVELOPMENT OF AN
OPTIMUM SYMMETRICAL NUMBER SYSTEM
DIRECTION FINDING ARRAY

by

Panayiotis Papandreou

March 1997

Thesis Co-Advisors: Phillip E. Pace
                                  David C. Jenn

1. AGENCY USE ONLY *(Leave blank)*	2. REPORT DATE March 1997	3. REPORT TYPE AND DATES COVERED Master's Thesis

4. TITLE AND SUBTITLE TITLE OF THESIS: DESIGN AND PROTOTYPE DEVELOPMENT OF A SYMMETRICAL NUMBER SYSTEM DIRECTION FINDING ARRAY	5. FUNDING NUMBERS

6. AUTHOR(S)
Papandreou Panayiotis

7. PERFORMING ORGANIZATION NAME(S) AND ADDRESS(ES) Naval Postgraduate School Monterey CA 93943-5000	8. PERFORMING ORGANIZATION REPORT NUMBER

9. SPONSORING/MONITORING AGENCY NAME AND ADDRESS Research and Development Office, Washington DC	10. SPONSORING/MONITORING AGENCY REPORT NUMBER

11. SUPPLEMENTARY NOTES The views expressed in this thesis are those of the author and do not reflect the official policy or position of the Department of Defense or the U.S. Government.

12a. DISTRIBUTION/AVAILABILITY STATEMENT Approved for public release; distribution is unlimited.	12b. DISTRIBUTION CODE

13. ABSTRACT *(maximum 200 words)*

One method of estimating the direction of an electromagnetic source is based on phase comparison. In this thesis the design and fabrication of a prototype antenna to demonstrate a new DF antenna architecture is described. Four antenna elements are grouped into three pairs with element spacing according to a set of symmetrical number system pairwise relatively prime moduli ($m_1 = 3$, $m_2 = 4$, $m_3 = 5$). The phase difference between each pair of elements is a symmetrical folding waveform that is determined using a mixer. The output voltage from each pair is amplitude analyzed using a small comparator ladder. In each channel, the symmetrically folding waveform, folds in accordance with the channel modulus and thus, only requires a precision according to that modulus. A high resolution DF is achieved after the N different SNS moduli are used and the results of these low-precision channels are recombined to yield the direction of arrival. The frequency of operation of the prototype is 8.5 GHz. Results based on measured and simulated data are presented.

14. SUBJECT TERMS. Direction Finding antennas, Symmetrical number Systems	15. NUMBER OF PAGES:
	16. PRICE CODE

17. SECURITY CLASSIFICATION OF REPORT Unclassified	18. SECURITY CLASSIFICATION OF THIS PAGE Unclassified	19. SECURITY CLASSIFICATION OF ABSTRACT Unclassified	20. LIMITATION OF ABSTRACT UL

DESIGN AND PROTOTYPE DEVELOPMENT OF AN OPTIMUM SYMMETRICAL NUMBER SYSTEM DIRECTION FINDING ARRAY

Panayiotis Papandreou
Lieutenant, Hellenic Navy
B.S., Hellenic Naval Academy, 1989

Submitted in partial fulfillment of the
requirements for the degree of

MASTER OF SCIENCE IN ELECTRICAL ENGINEERING

from the

NAVAL POSTGRADUATE SCHOOL

March 1997

ABSTRACT

One method of estimating the direction of an electromagnetic source is based on phase comparison. In this thesis the design and fabrication of a prototype antenna to demonstrate a new DF antenna architecture is described. Four antenna elements are grouped into three pairs with element spacing according to a set of symmetrical number system pairwise relatively prime moduli ($m_1 = 3$, $m_2 = 4$, $m_3 = 5$). The phase difference between each pair of elements is a symmetrical folding waveform that is determined using a mixer. The output voltage from each pair is amplitude analyzed using a small comparator ladder. In each channel, the symmetrically folding waveform, folds in accordance with the channel modulus and thus, only requires a precision according to that modulus. A high resolution DF is achieved after the N different SNS moduli are used and the results of these low-precision channels are recombined to yield the direction of arrival. The frequency of operation of the prototype is 8.5 GHz. Results based on measured and simulated data are presented.

TABLE OF CONTENTS

LIST OF FIGURES

LIST OF TABLES

ACKNOWLEDGEMENTS

I. INTRODUCTION

A. DIRECTION FINDING SYSTEMS

A radio direction finder (RDF) is a passive device that determines the direction of arrival (DOA) of electromagnetic energy. No transmission of electromagnetic energy by the RDF is involved; it is a passive receiving system. It receives the incident electromagnetic wave, processes the received signal, and thereby determines the direction of the source. Although the radio direction finding, i.e. the use of an RDF in finding the direction of a radio source, is only a class of direction finding, often the broad term is used in the narrow sense.

The importance of the information provided by a direction finding (DF) system, the emitter's bearing, is significant in several applications. For example, based on this information the identification of a communication system or of a radar can be performed. Also, the use of active electromagnetic counter measures (ECM) against an electromagnetic source, requires an electronic warfare support system to measure the direction to the victim.

A radio direction finder consists of four essential functional elements as depicted in Figure 1.1. The antenna extracts electromagnetic energy and converts it to a signal containing direction-of-arrival information. The receiver converts, amplifies, and processes the signal to an intermediate frequency (IF) or baseband. The postreceiver processor further processes the signal to obtain basic DOA information, and the DF

1

```
                    ┌─────────────────────────┐
                    │       RF   ENERGY        │
                    │    INCIDENT  AT  SOME    │
                    │   DIRECTION-OF-ARRIVAL   │
                    └─────────────────────────┘
                                │
        ┌───────────────────────┼──────────────────────────┐
        │                       ▼                           │
        │           ┌─────────────────────────┐             │
        │           │        ANTENNA          │             │
        │           │   WITH   DIRECTIONAL    │             │
        │           │    CHARACTERISTICS      │             │
        │           └─────────────────────────┘             │
        │                       │                           │
        │                       ▼                           │
        │           ┌─────────────────────────┐             │
        │           │    RECEIVER  FOR        │             │
   RDF  │           │   RF / IF  BASEBAND     │             │
        │           │     PROCESSING          │             │
        │           └─────────────────────────┘             │
        │                       │                           │
        │                       ▼                           │
        │           ┌─────────────────────────┐             │
        │           │    POST   RECEIVER      │             │
        │           │   PROCESSING  FOR       │             │
        │           │   DF  INFORMATION       │             │
        │           └─────────────────────────┘             │
        │                       │                           │
        │                       ▼                           │
        │           ┌─────────────────────────┐             │
        │           │  DIRECTION-OF-ARRIVAL   │             │
        │           │     INFORMATION         │             │
        │           └─────────────────────────┘             │
        │                       │                           │
        └───────────────────────┼──────────────────────────┘
                                ▼
                    ┌─────────────────────────┐
                    │   DF  INFORMATION       │
                    │   PROCESSING            │
                    │   READ-OUT  DISPLAY     │
                    └─────────────────────────┘
```
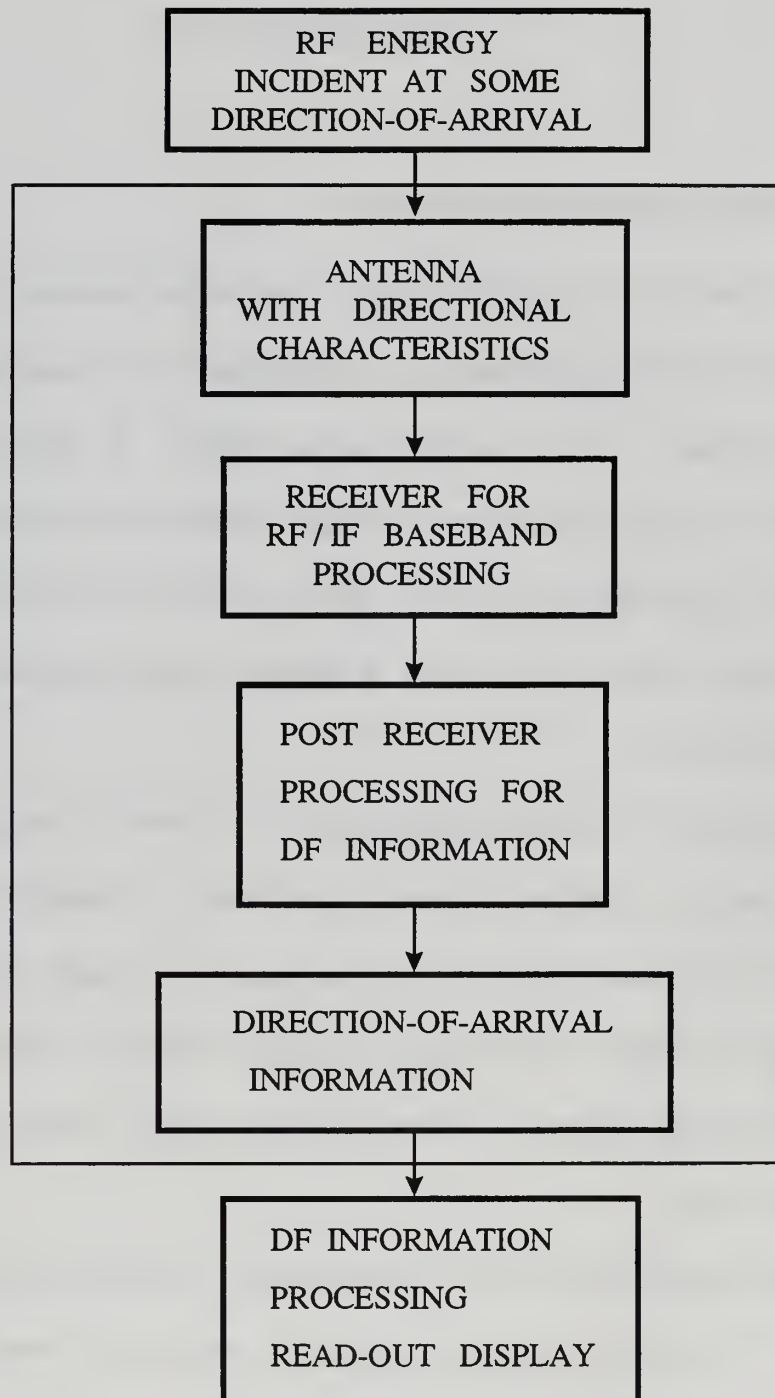
Figure 1.1: Functional elements of the direction finding process.

information processing-read-out-display unit prepares the basic DOA data for transmission to users of the DF information [Ref 1].

Desirable characteristics of a DF system include: (1) wide instantaneous bandwidth, (2) high speed, (3) minimum number of antenna elements, (4) high resolution, and (5) wide instantaneous field of view. The antenna is a critical component of a DF system, and frequently is the limiting factor in the system performance. It has been difficult for traditional antenna architectures to achieve all of these attributes simultaneously.

The DF systems are separated into three categories according to their aperture. They are: small-aperture (or narrow-aperture), medium-aperture, and large-aperture (or wide-aperture). Although the boundaries between them are not well specified, and some "gray" areas occur, small-aperture systems generally have their aperture equal to half the wavelength of the highest frequency, while the large-aperture region is considered to start from about two times the wavelength. Medium-aperture systems are considered to start from 0.2 to 1.2 wavelengths.

The direction of arrival is mainly determined by one of three methods: (1) amplitude response, (2) phase delay, or (3) time delay. In all three methods the angle of arrival of the electromagnetic wave is converted into DC voltage, although the technique for interpreting the voltage is different in each case.

The amplitude response method mainly uses dipole-like antenna patterns to obtain the DF information. A radiation pattern of a dipole looks like an "eight;" it is broad at the maximum and sharp at the minimum. By rotating the dipole it is possible to find the direction of the emitter with a relatively high accuracy; it will be the null position, where

the voltage at the antenna terminals goes to zero. There is a 180 degree ambiguity, because of the pattern symmetry, which can be resolved by a second antenna with a cardioid pattern. If mechanical rotation of the dipole is not easy to accomplish, two dipoles positioned so as to give orthogonal patterns can be used. The values of the electric field for the two dipoles are measured and converted to voltages which are proportional to the sine and cosine of the incident angle, which provide angle information.

For the phase delay method at least two separate antenna elements with a predetermined space between them are required. Since the distances from the emitter to the two elements are not the same (except the symmetric case), the incident wave arrives at the two elements after traveling uneven paths, and thus it arrives with a different phase. The phase delay is proportional to the spacing, the wavelength, and the angle of incidence. Since the first two factors are constant, the DF information can be obtained.

Similarly the third method, time delay, uses at least two antenna elements. The electromagnetic wave arrives at the two elements at different times. The time difference is proportional to the distance between the antennas (which is predetermined and constant), and the angle of incidence. Thus the direction of the emitter is obtained.

All three methods contain ambiguities and limitations, which vary for each case. Also we have to keep in mind that the direction finding procedure is subject to several kinds of errors, which can accumulate under certain circumstances. They include propagation-induced errors caused by the propagation medium which introduces deviations to the signal, environmental errors from sources in the vicinity of the direction

finder that scatter or reradiate the signal, measurement errors caused by instrument imperfections, and observational errors.

B. PRINCIPAL CONTRIBUTIONS

This thesis is concerned with direction finders that use the phase delay method to find the direction of an emitter. In particular, it deals with the construction of a medium aperture radio direction finder that operates up to the frequency of 8.5 GHz and incorporates a new signal processing approach based on symmetric number systems (SNS). It also demonstrates how the ambiguities that occur with this method can be overcome.

This system contains four separate antenna elements: one primary and three secondary. The output of the primary element is mixed with the output of each of the three secondary elements thus forming three output channels. The phase difference between the primary and the secondary in each case is converted to a voltage. The output phase signals are symmetrically folding waveforms that are amplitude analyzed by a small group of comparators. In each channel, the symmetrically folding waveform, folds in accordance with the channel modulus and thus, only requires a precision according to that modulus. A high resolution DF is achieved after the N different SNS moduli are used and the results of these low-precision channels are recombined to yield the direction of arrival.

It is shown that the direction of arrival is given uniquely by the set of integer values determined by the number of comparator threshold crossings for each modulus. The resulting angle of arrival estimates contain quantization error, which increases with

the angle off of the electrical boresight. This is analogous to the increase in beamwidth for an array that is scanned electronically. Several other sources of error exist: frequency scanning error, when the emitter uses a frequency other than the design frequency, and inaccurate comparator threshold settings.

The objective of this research is to experimentally investigate the fundamental DF antenna concepts by building a prototype and measuring its performance in the anechoic chamber. To reduce cost, off-the-shelf in-house hardware is used in the array. Therefore, the array performance is not the optimum, but the array can be used to validate the important SNS DF concepts. A simple narrow band radiating element is used. The SNS DF antenna is designed for use with an existing comparator and encoding hardware developed on a previous research program.

The wide-band performance of the array is primarily determined by the radiating element design, which will not be addressed in this research. All of the fundamental concepts can be demonstrated using narrow band elements. They include: (1) microwave beamforming network design and the performance requirements of its components (mixers and amplifiers), (2) DF resolution as a function of angle, (3) effect of the element factor and signal-to-noise (SNR) level on DF accuracy, (4) resolution versus boresight, (5) interface between each channel's phase response and the corresponding amplitude analyzing hardware, and (6) verification of frequency compensation and interpolation methods to maintain high resolution.

C. THESIS OUTLINE

The thesis presents the theoretical background and the design equations needed to construct a large aperture radio direction finder based on a symmetric number system. A DF array was fabricated, assembled and measured in the anechoic chamber. The measured data verified the fundamental concept and performance of the new SNS DF approach.

Chapter II presents a theoretical background in direction finders using the phase difference between antenna elements for direction of arrival information. A design for a 8.5 GHz four-element array is presented. Chapter III describes the actual design and the fabrication of the direction finding system. It begins with the process of component evaluation in the lab. Individual antenna components such as the mixers and the low noise amplifiers were measured on the network analyzer so that differences in their phases and amplitudes could be compensated for in the actual design. Next the design and assembly of the system follows. This includes phase trimming and checkout in the lab. A plane wave was simulated by exciting both branches with equal amplitude signals that had known phase differences to verify the assembly before proceeding to the chamber. Chapter IV presents the experimental anechoic chamber results, and Chapter V states some conclusions and recommendations for future research.

II. PHASE COMPARISON DF SYSTEMS

A. OVERVIEW

Phase comparison DF systems consist of several antenna elements which are arranged in a particular geometrical configuration. The number of the elements and arrangement depends on the DOAs of interest and the method used to process the signals. However, the minimum number of elements is two. The determination of DOA is performed by direct phase comparison of the received signals from the different antenna elements.

Figure 2.1 shows the geometry of a typical two element system. The two antenna elements define a line, here the x-axis, and they are separated by a distance d, the baseline spacing. The x-y plane corresponds to the earth's surface for a ground based system, with the z axis the vertical axis. The source is assumed to be far away, so the wavefronts of the incident signal are planar, and the wave arrives at the same angle at both antenna elements. The bearing of the incident wave φ_B, is measured in the horizontal x-y plane from the y axis, while the elevation angle θ, which for the general case is not 90 degrees, is measured from the z axis towards the x-y plane.

For a linear array, only for the case where $\varphi_B = 0$ does the incident wave arrive at the same time at all antenna elements. For all the other cases the wave arrives at different time instances at the two antenna elements due to unequal paths from the source. This time difference of arrival is a function of the angle φ_B. Therefore, every horizontal bearing φ_B is related to a certain time or path difference. Also, the phase of a traveling
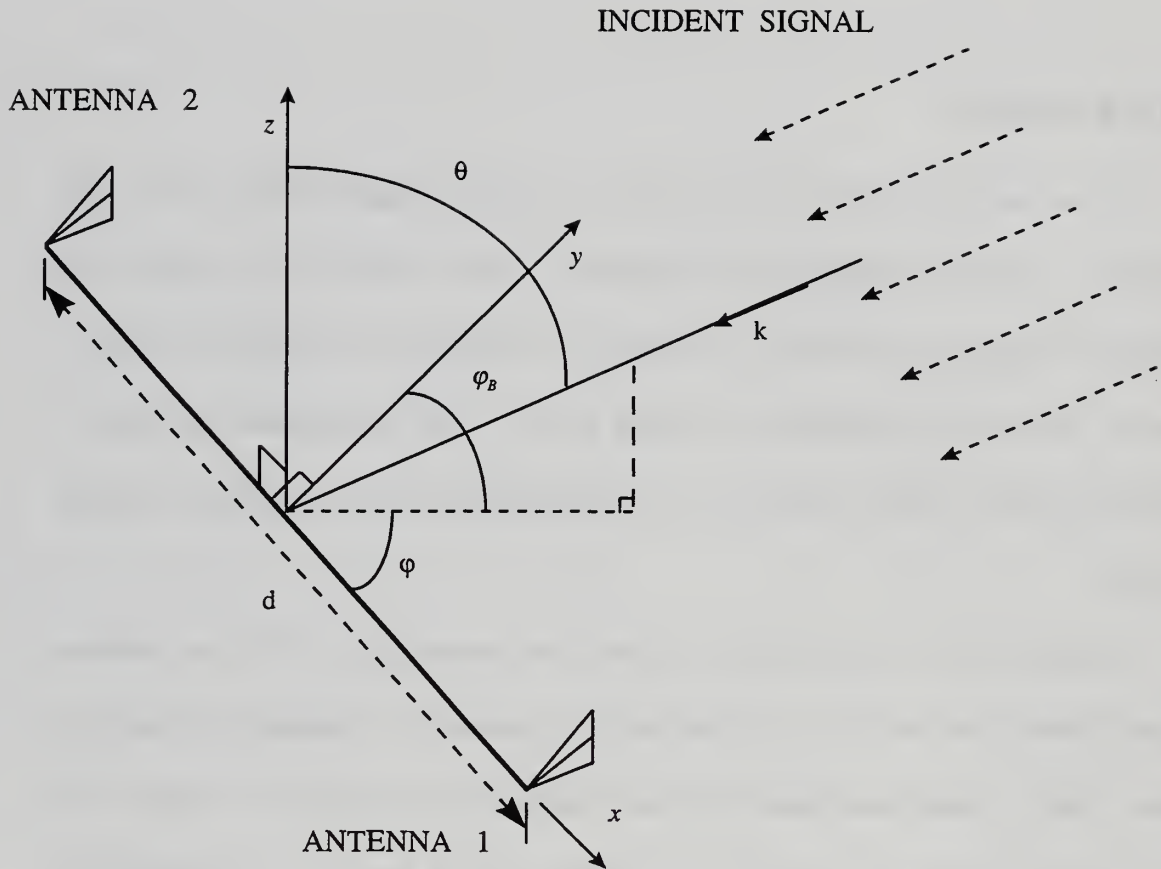
Figure 2.1: Geometry of phase comparison DF.

electromagnetic wave changes periodically in a sinusoidal way. This means that the incident wave will arrive at each of the antenna elements with a certain phase that corresponds to the distance (or the time) that the wave has traveled. Thus any time or path difference is associated with a certain phase difference.

Figure 2.2 shows the functional components of the direction finding array. The incident electromagnetic wave causes an sinusoidal voltage of the same frequency at the output of the antenna. Each element is connected with a cable to the input of a mixer,

which operates as a phase comparator. With equal cable lengths the two signals arrive at the input of the mixer with the free space (plane wave) phase difference. At the mixer the two AC voltages are multiplied and at the output they produce a voltage which is a function of the phase difference of the incident wavefront. Thus an azimuthal angle of
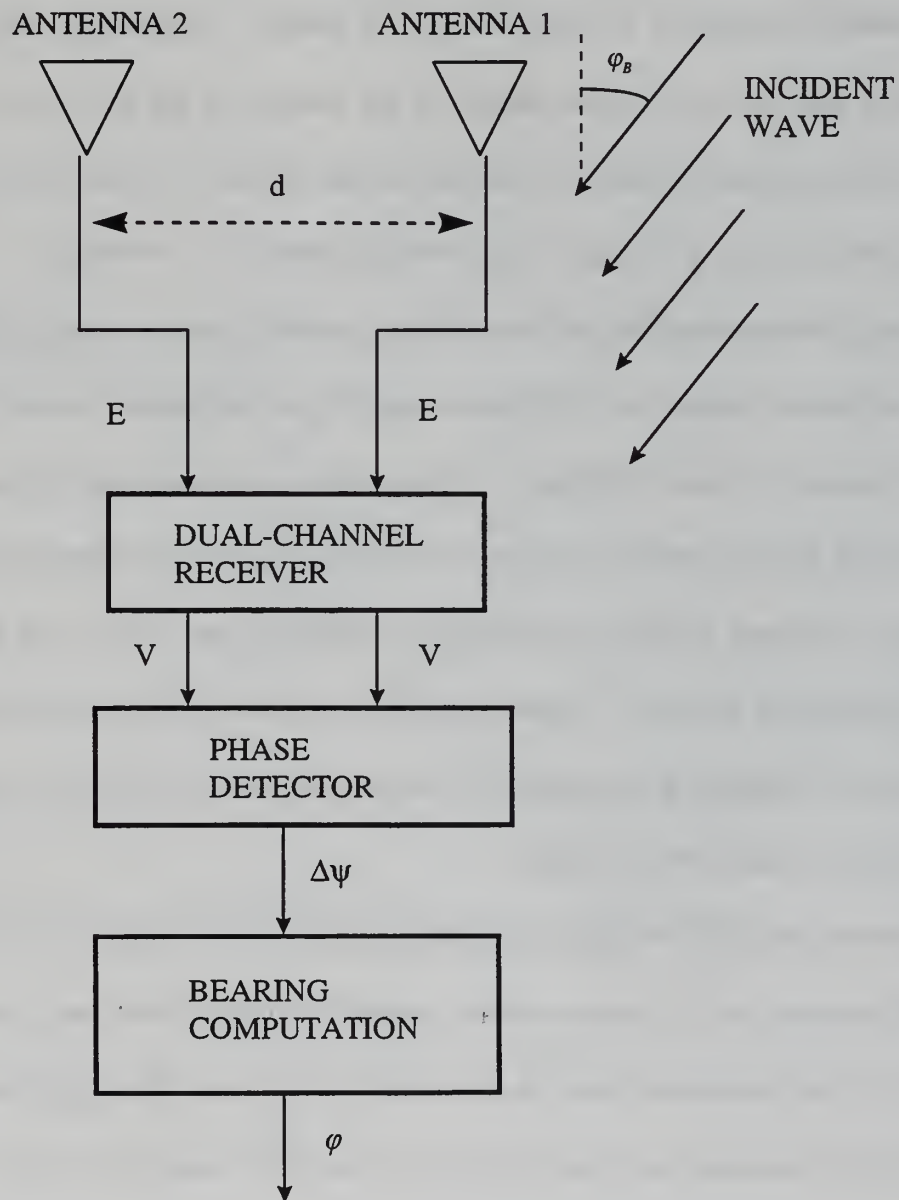
Figure 2.2: Phase comparison using a single-baseline antenna and a dual channel receiver.

incidence φ_B causes a certain time (or distance-traveled) difference between the two antenna elements, and equivalently a certain phase difference between the two elements that corresponds to a certain voltage value, which is measured.

In order to have unambiguous AOA estimates from -90 to +90 degrees, the phase difference must correspond to a range of $-\pi$ to π radians. Having φ_B equal to 90 degrees means that the wave travels parallel to the baseline of the two elements, and therefore d is the additional distance to reach the second element. In order to arrive there with a phase difference of π radians d must be equal to half of a wavelength.

Although this approach avoids the ambiguity problem, there is a tradeoff: there is a limit to resolution, because the 180 degree range of possible source bearings cannot exceed 2π radians of phase difference. There is also a second consideration. The distance between the two elements is going to be half the wavelength this means that for the frequency of interest, 8.5 GHz, this distance is about 1.76 cm. This is too close for most types of radiating elements. A better approach is to place the antenna elements at a distance equal to a multiple of the half the wavelength, and then use multiple arrays with different spacings to resolve the ambiguity.

Estimating the elevation angle θ is a separate issue. For a single baseline system all elevation angles give the same antenna response, and thus it is not possible to determine θ. The elevation angle can be determined with the use of a second baseline, if the second pair of elements is placed orthogonal to the first, i.e. along the vertical axis. This yields a set of two independent measurements, which correspond to the two angles φ_B and θ. However, the estimation of θ will not be a subject of this thesis. In this case we restrict both the antenna and the signal source to lie in the x-y plane.

B. THEORETICAL APPROACH

The purpose of this section is to present the mathematical approach and derive the equations that relate angle of incidence with phase difference at the elements to the voltage at the output of the mixer. Figure 2.3 shows the geometry of the problem. As
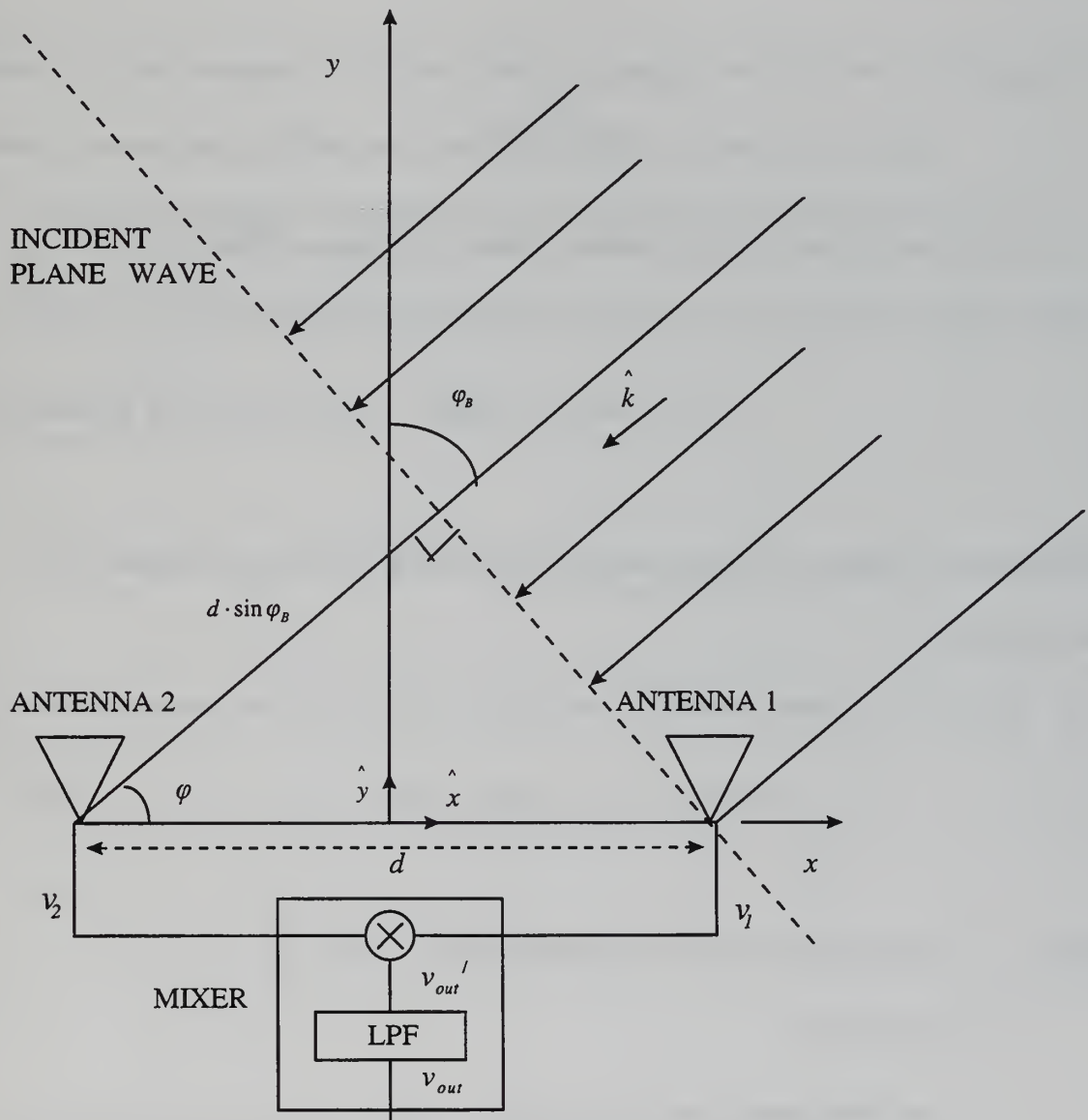
Figure2.3: Linear array geometry.

mentioned previously, the elevation angle is 90 degrees and we consider only waves arriving in the x-y plane. There are two antenna elements with distance d, and the plane wave travels with incidence angle φ_B. The angle φ_B is measured from the perpendicular to the baseline axis and it takes values from $+\pi/2$ to $-\pi/2$. Note that φ_B is related to the spherical polar angle φ by:

$$\varphi_B = \frac{\pi}{2} - \varphi$$

Let $\hat{k}$ be the unit vector of the direction of wave propagation. Then

$$\hat{k} = -(\hat{x} \cdot \cos\varphi + \hat{y} \cdot \sin\varphi) \tag{2.1}$$

The instantaneous electric field propagating toward the array in free space is given by the following formula:

$$E(t,k) = \hat{z} \cdot E_0 \cdot \cos(2\pi f t - \beta r) \tag{2.2}$$

where : E_0 is the maximum value of the electric field,

   f is the frequency

   β is the phase constant (or wave number)

   r is the distance traveled from source

$$\beta r = -\beta(x \cdot \sin\varphi_B + y \cdot \cos\varphi_B)$$

and we assume that the wave is vertically polarized. The phase constant β is equal to

$$\beta = \frac{2\pi}{\lambda} \qquad (2.3)$$

where λ is the wavelength. This last relationship implies that for every wavelength of distance traveled, an equiphase plane undergoes a phase change of 2π radians.

The electromagnetic wave arrives first at the element 1. This element is located at $x = \frac{d}{2}$ and $y = 0$. Without affecting the general case, we can assume that the phase of the wave arriving there at time t is

$$\psi_1 = 2\pi f t \qquad (2.4)$$

The wave arrives at element 2 after traveling an additional distance of $d \cdot \sin\varphi_B$. Its phase is

$$\psi_2 = 2\pi f t - \frac{2\pi}{\lambda} \cdot d \cdot \sin\varphi_B \qquad (2.5)$$

From (2.4) and (2.5), the phase difference between the two elements is:

$$\Delta\psi = \psi_1 - \psi_2$$

$$= 2\pi ft - (2\pi ft - \frac{2\pi}{\lambda} \cdot d \cdot \sin\varphi_B)$$

$$\Delta\psi = 2\pi \cdot \frac{d}{\lambda} \cdot \sin\varphi_B \qquad\qquad (2.6)$$

The last equation presents the relationship between angle of incidence of the electromagnetic wave and phase difference between the two elements $\Delta\psi$.

The signals received by the antenna elements are fed to a mixer. A mixer multiplies its two input signals and passes the product through a low pass filter. The output is a signal whose frequency is the difference of the two input signals' frequencies. If they have the same frequency, then the output is a voltage whose value proportional to the phase difference. The two signals at the mixer in this case are two sinusoidal signals of the same frequency (8.5 GHz), but with different phases α_1 and α_2. These input phases are not purely ψ_1 and ψ_2 because of the phase delays due to the lengths of the wiring from the antenna to the mixer. Each branch introduces a constant phase shift which is added to the phase at the respective elements. The phase shifts generally are different, but their difference is constant ψ_0 which can be measured. Thus the phase difference $\Delta\alpha$ at the input of mixer can be calculated from

$$\Delta\alpha = \Delta\psi + \psi_0 \qquad\qquad (2.7)$$

Alternately, if we choose the length of the cable to be equal for both branches, $\Delta\alpha = \Delta\psi$.

The latter approach of equal paths is preferred, but sometimes is not possible to achieve because of the circuit layout constraints.

The two inputs of the mixer are of the form

$$v_1(t) = V \cdot \cos[2\pi f t + \alpha_1(t)] \tag{2.8a}$$

$$v_2(t) = V \cdot \cos[2\pi f t + \alpha_2(t)] \tag{2.8b}$$

where, V is the maximum value of the voltage at the element terminals due to the incident wave, and f is the frequency of 8.5 GHz. Before low pass filtering the instantaneous mixer output voltage is

$$v_{out}'(t) = v_1(t) \cdot v_2(t)$$

$$v_{out}'(t) = V^2 \cdot \cos[2\pi f t + \alpha_1(t)] \cdot \cos[2\pi f t + \alpha_2(t)]$$

$$v_{out}'(t) = \frac{V^2}{2} \cdot \{\cos[4\pi f t + \alpha_1(t) + \alpha_2(t)] + \cos[\alpha_1(t) - \alpha_2(t)]\} \tag{2.9}$$

The low pass filtering removes the high frequency term on the right hand side of (2.9) leaving

$$v_{out}(t) = \frac{V^2}{2} \cdot \cos[\alpha_1(t) - \alpha_2(t)]$$

$$v_{out}(t) = \frac{V^2}{2} \cdot \cos(\Delta\alpha)$$

$$v_{out}(t) = \frac{V^2}{2} \cdot \cos(\Delta\psi) \tag{2.10}$$

which is the required voltage. Equation (2.10) presents the relationship between the mixer voltage output v_{out} and phase difference at the elements. Combining equations (2.6) and (2.10) gives

$$v_{out}(t) = \frac{V^2}{2} \cdot \cos[2\pi \cdot \frac{d}{\lambda} \cdot \sin(\varphi_B)] \tag{2.11}$$

Equation (2.11) is the relationship between voltage at the output of the mixer and angle of incidence of the electromagnetic wave.

From Equation (2.6) it is apparent that if the baseline d is half the wavelength λ or less, the phase difference is between $-\pi$ and π. For every value of phase difference there is only one unique angle of incidence. In this case no ambiguities exist. With distance between the two elements half the wavelength, the phase difference is

$$\Delta\psi = \pi \cdot \sin(\varphi_B) \tag{2.12}$$

and it is plotted in Figure 2.4. Figure 2.5 shows the plot of Equation (2.10); the voltage versus phase difference. Note that this plot is independent of the baseline length
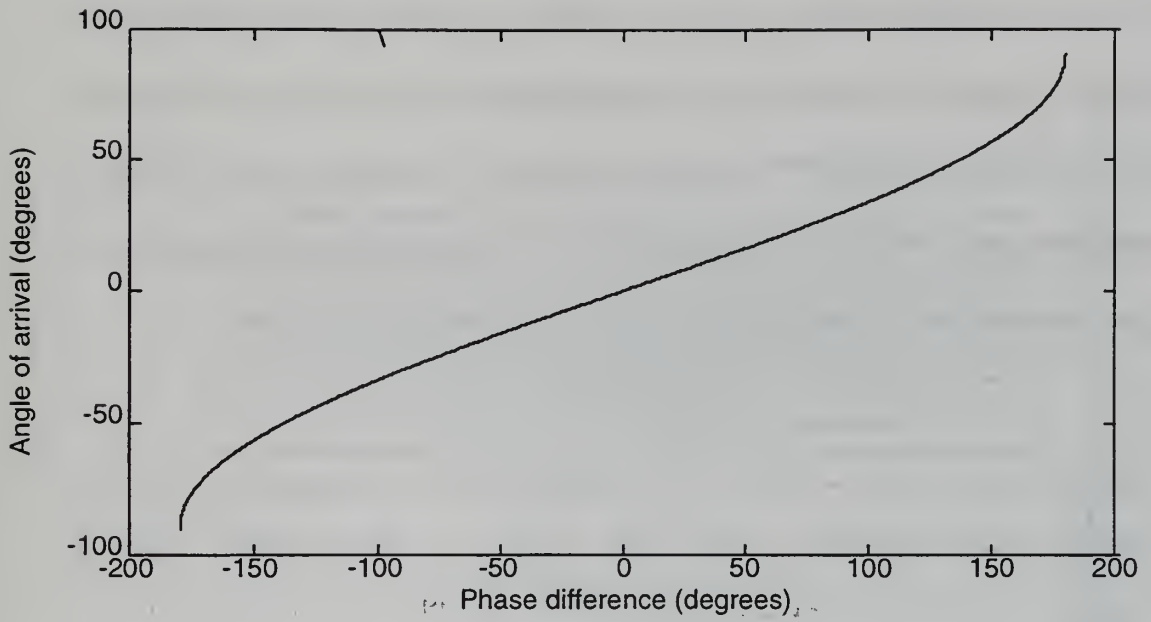
Figure 2.4: Angle of arrival vs phase difference at the elements for $d = \dfrac{\lambda}{2}$.
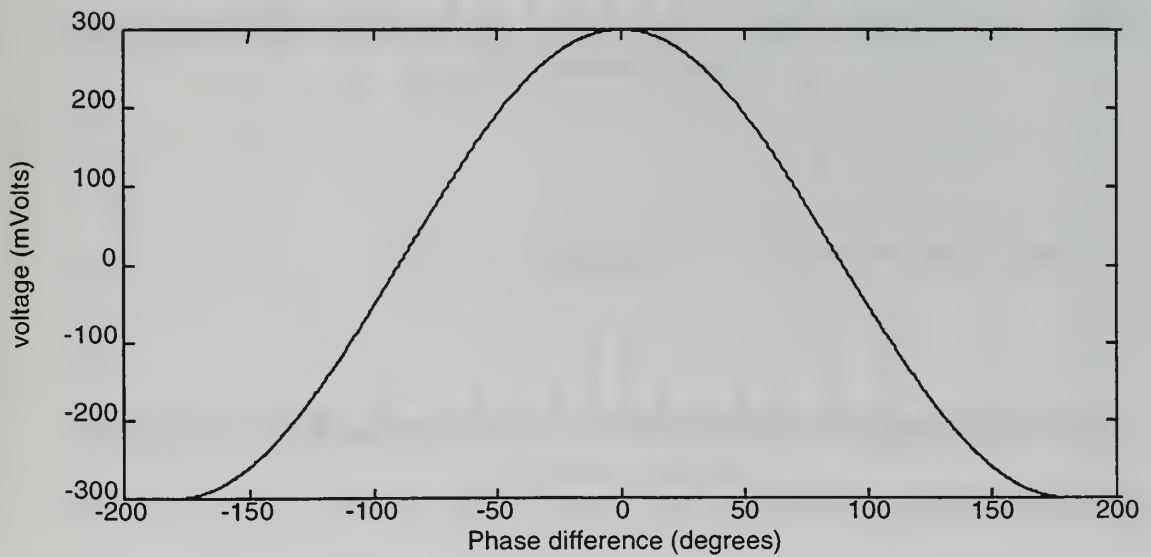
Figure 2.5: Phase difference at the elements vs mixer output voltage for $d = \dfrac{\lambda}{2}$.

and is the same for every baseline. For every voltage value there are two possible phase differences: ψ and $-\psi$. Figure 2.6 is a direct combination of the curves in Figures 2.4 and 2.5; it is the plot of voltage versus angle of incidence. For every value of voltage we have only two possible values of angle of incidence. This ambiguity can be eliminated by using a second array with a baseline that is not an integer multiple of the first.
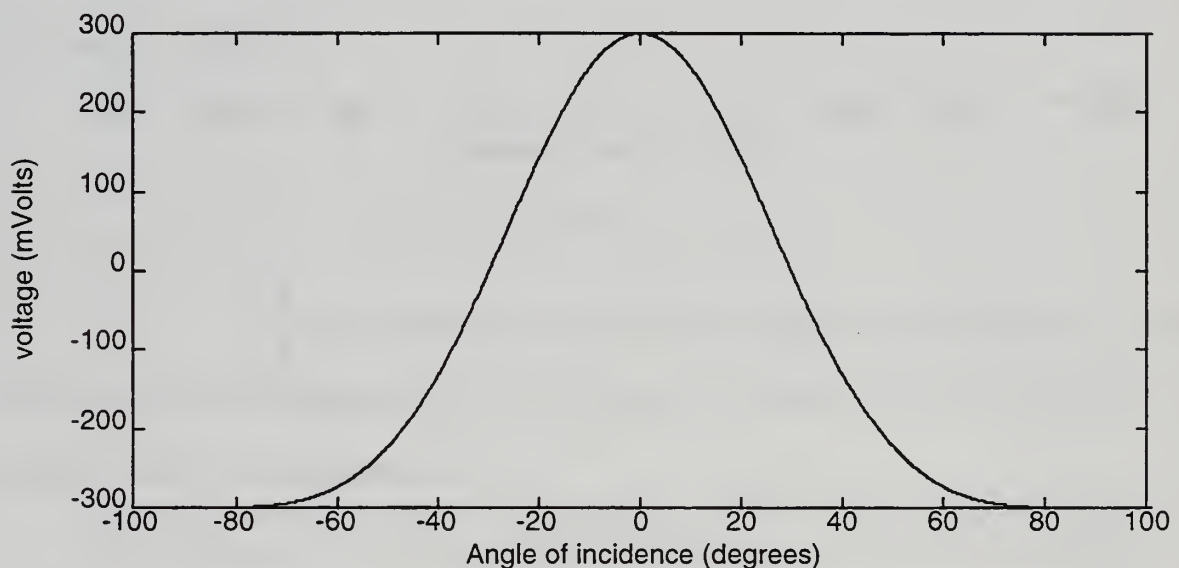
Figure 2.6: Angle of arrival vs mixer output voltage for $d = \dfrac{\lambda}{2}$.

For baselines greater than half the wavelength more ambiguities exist, since the phase difference takes on multiple values outside of the interval $-\pi$ to π, and thus corresponds to more than one angle of incidence. Figures 2.7 and 2.8 show the data for a baseline d equal to 7.5 times the wavelength. The rapid change in voltage with phase
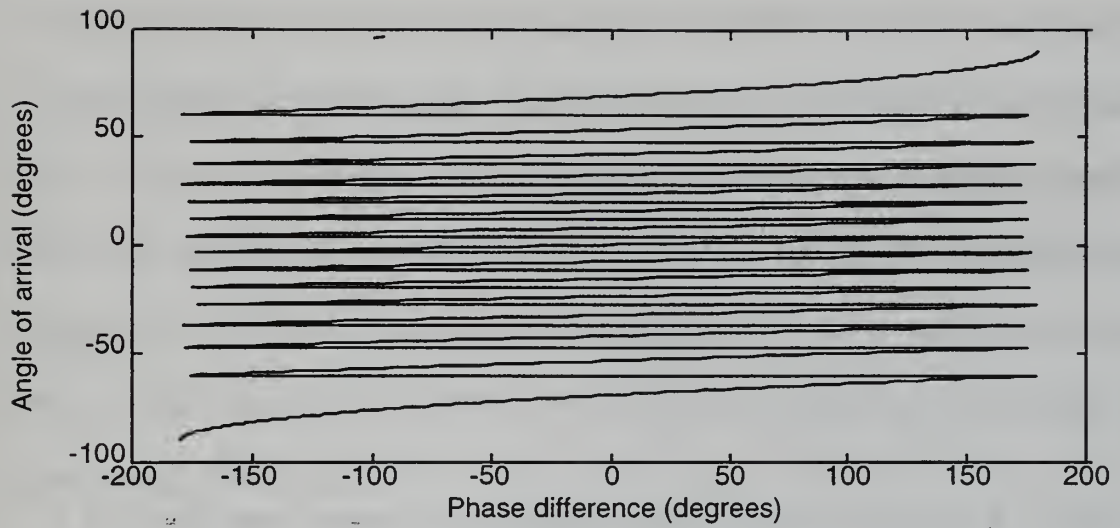
Figure 2.7: Angle of arrival vs phase difference for $d = 7.5\lambda$.
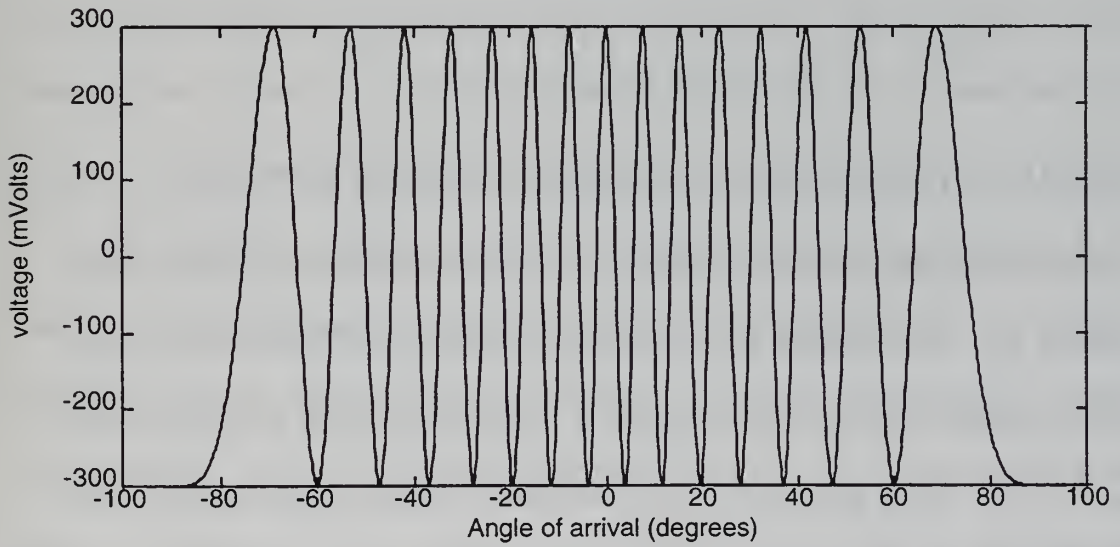
Figure 2.8: Angle of arrival vs mixer output voltage for $d = 7.5\lambda$.

21

difference allows higher resolution AOA estimates. The tradeoff is that the voltage is highly ambiguous; 15 angles of incidence correspond to every value of phase difference, and 30 angles of incidence to every value of voltage. The number of periods n that correspond to 180 degrees in a voltage versus angle plot is

$$n = \frac{2d}{\lambda} \qquad (2.13)$$

Figure 2.8 illustrates that the voltage period is not constant when plotted as a function of angle. The period increases with the increase of DOA from the array broadside ($\varphi_B = 0$) because of the $\sin \varphi_B$ dependence in Equation (2.6). This is the same reason that the beamwidth of an electronically scanned phased array increases with scan angle.

C. OPTIMUM SYMMETRICAL NUMBER SYSTEM ANTENNA

The optimum SNS scheme is composed of a number of pairwise relatively prime (PRP) moduli m_i. The integers within each SNS modulus are representative of a symmetrically folded waveform with the period of the waveform equal to twice the PRP modulus, i.e., $2m_i$. For m given, the integer values within twice the individual modulus are given by the row vector

$$x_m = [0,1,...,m-1,m-1,...,1,0].$$

From this expression, the required number of comparators for each channel is m_i-1. Due to the presence of ambiguities, the integers within the vector do not form a complete system of length $2m$ by themselves. The ambiguities that arise within the modulus are resolved by considering the paired values from all channels together. By recombining the N channels, the SNS is rendered a complete system having a one-to-one correspondence with the residue number system (RNS). For N equal to the number of PRP moduli, the dynamic range of this scheme is

$$M = \prod_{i=1}^{N} m_i .$$

This dynamic range is also the position of the first repetitive moduli vector. For the example of $m_1 = 4$ and $m_2 = 3$, the first repetitive moduli vector occurs at an input of 12 [Ref 6].

The ambiguity problem observed in Figure 2.8 can be eliminated by the simultaneous use of more than one pair of antenna elements with differing baselines of several wavelengths depending upon the modulus with each pair forming a separate receive channel. The output of each channel or modulus is amplitude analyzed by a small ladder of comparators. The channels are recombined and the result is a high accuracy unambiguous estimate of the DOA.

Consider the case of two pairs of antenna elements with different baselines. The plots of the voltage at each mixer output versus angle of arrival is a sinusoid. In order to

convert these analog signals to digital codes, they are quantized with respect to predefined reference levels (see Figure 2.9). Each level represents an integer value within the modulus. The number of possible digits m is the number of the reference levels n plus one. If the first signal is quantized with two reference levels and the second with three, they are converted to the two strings shown in Table 2.1.
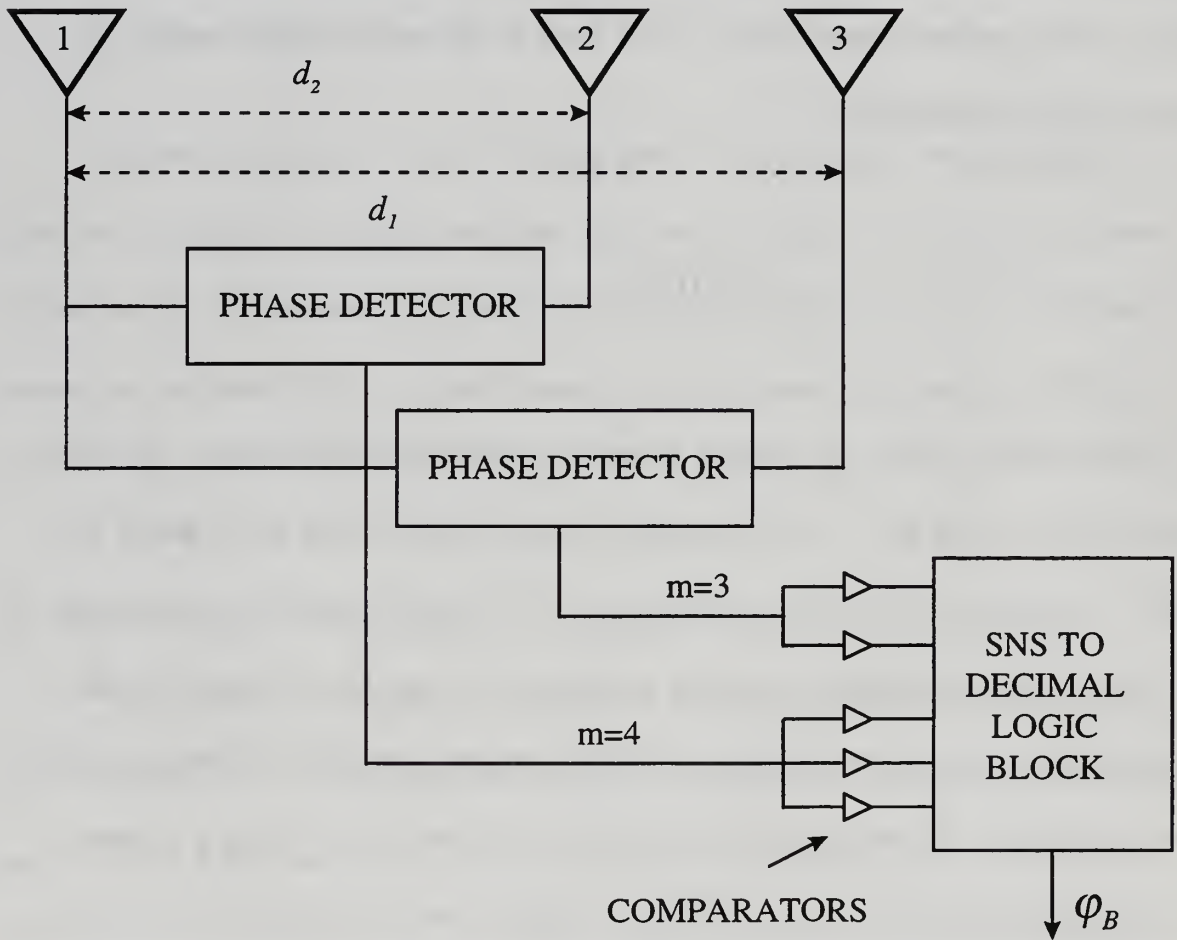
Figure 2.9: Optimum SNS antenna architecture using 2 moduli ($m_1 = 3$, $m_2 = 4$).

	$m_1 = 3$	$m_2 = 4$
Angle Interval	3 digits / 2 reference levels	4 digits/3 reference levels
1	0	0
2	1	1
3	2	2
4	2	3
5	1	3
6	0	2
7	0	1
8	1	0
9	2	0
10	2	1
11	1	2
12	0	3
13	0	3

Table 2.1: Example of quantization of symmetrical waveforms with 2 and 3 reference levels.

The entries in Table 2.1 are the possible values that an incoming signal produces at the output of the comparator ladder for each baseline. They are periodic with different periods for each case (period is $2m_i$). If they are viewed as pairs, the first twelve of them are unambiguous: none of them appears twice. Note that this number is the product of

the possible digits m_i for the two cases ($M = m_1 \cdot m_2 = 3 \cdot 4 = 12$), and is called dynamic range. If within the dynamic range both plots cover exactly 180 degrees, then each table entry corresponds to a 15 degrees interval. Thus, by knowing the two digits we know the angle of arrival. However, since the voltage is quantized, the DOA estimate is also quantized. Therefore the DOA can only be determined with a certain resolution. The difference between the estimate and the true DOA is the quantization error.

Within the dynamic range the first column of integers has $n_1 = 2$ periods, while the second has $n_2 = 3/2$. From Equation (2.13) the required spacings for the unambiguous DOA estimates are

$$d_1 = \frac{n_1}{2} \lambda = \lambda$$
$$d_2 = \frac{n_2}{2} \lambda = 0.75 \cdot \lambda$$

(2.14)

Thus, two pairs of elements with these baselines having two and three quantization levels, respectively, yield unambiguous angle of arrival estimates with a resolution of 15°. Figure 2.10 shows the voltage at the mixer outputs for the two arrays versus angle of arrival, before and after quantization. All the resulting pairs of digits are unique. The above example has demonstrated that we can obtain unambiguous results if we use two arrays with the appropriate combination of spacings and quantization levels. The number of periods within the dynamic range is given by the following equation:

$$n_i = \frac{M}{2m_i} \qquad (2.15)$$

The number of periods in the phase waveform within 180 degrees is given by Equation (2.13). The condition for uniqueness that must be satisfied is that the integer in Equations
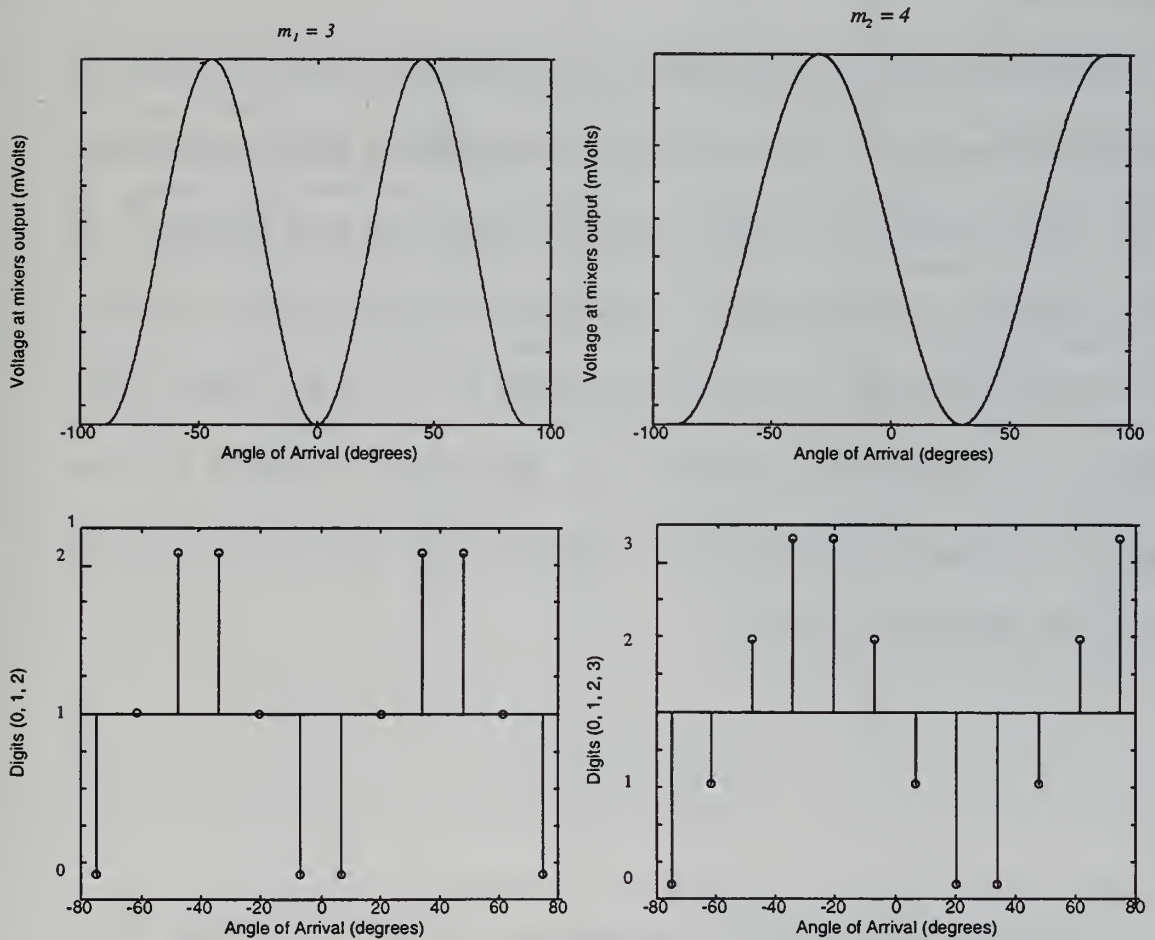
Figure 2.10: (a) Plots of the mixer outputs vs angle of arrival for the two baselines, and (b) digitization of the two plots in (a). Note that the pairs of digits are unambiguous.

(2.13) and (2.15) must be the same

$$n_1 = \frac{2d_1}{\lambda} = \frac{M}{2m_1} \qquad \text{(2.16a)}$$

$$n_2 = \frac{2d_2}{\lambda} = \frac{M}{2m_2} \qquad \text{(2.16b)}$$

with $M = m_1 \cdot m_2$.

Because of the $\sin \varphi_B$ term in Equation (2.6) the angle of arrival code widths are not uniform over the range of $-\pi$ to π. Therefore the resolution is greater near broadside ($\varphi_B = 0^\circ$) than at endfire ($\varphi_B = \pm 90^\circ$). For the example we have discussed the resolution is relatively poor (15 degrees). The resolution is determined by M. Resolution can be increased by adding more arrays or increasing the m_i for the existing arrays. Increasing the m_i requires more comparators for digitization. To increase M in our example we add a third pair of elements with 4 reference levels. The results are shown in Table 2.2. The dynamic range is now

$$M = m_1 \cdot m_2 \cdot m_3 = 60 \qquad \text{(2.17)}$$

The number of periods within the dynamic range are 10, 7.5 and 6 respectively, and the appropriate baseline lengths are the following:

Angle interval	$m_1 = 3$	$m_2 = 4$	$m_3 = 5$
	3 digits/ 2 ref. levels	4 digits/3 ref.levels	5 digits/ 4 ref. levels
1	0	0	0
2	1	1	1
3	2	2	2
4	2	3	3
5	1	3	4
6	0	2	4
7	0	1	3
8	1	0	2
9	2	0	1
10	2	1	0
11	1	2	0
12	0	3	1
13	0	3	2
14	1	2	3
15	2	1	4
$\vdots$	$\vdots$	$\vdots$	$\vdots$
58	2	1	2
59	1	2	1
60	0	3	0

Table 2.2: Quantization of symmetrical waveforms with 2,3, and 4 reference levels.

$$n_1 = \frac{2d_1}{\lambda} \Rightarrow d_1 = \frac{n_1}{2} \cdot \lambda = 5\lambda \qquad (2.18a)$$

$$n_2 = \frac{2d_2}{\lambda} \Rightarrow d_2 = \frac{n_2}{2} \cdot \lambda = 375\lambda \qquad (2.18b)$$

$$n_1 = \frac{2d_1}{\lambda} \Rightarrow d_1 = \frac{n_1}{2} \cdot \lambda \Rightarrow d_1 = 3\lambda \qquad (2.18c)$$

Figure 2.11 shows the plots before and after the quantization for the three cases. Since the 180 degrees are divided to 60 intervals, the resolution is 3 degrees at broadside. As Equations (2.16) suggest, the desired resolution can be achieved with several different combinations. Resolution is a tradeoff between number of arrays (element pairs) and number of quantization levels (comparators).
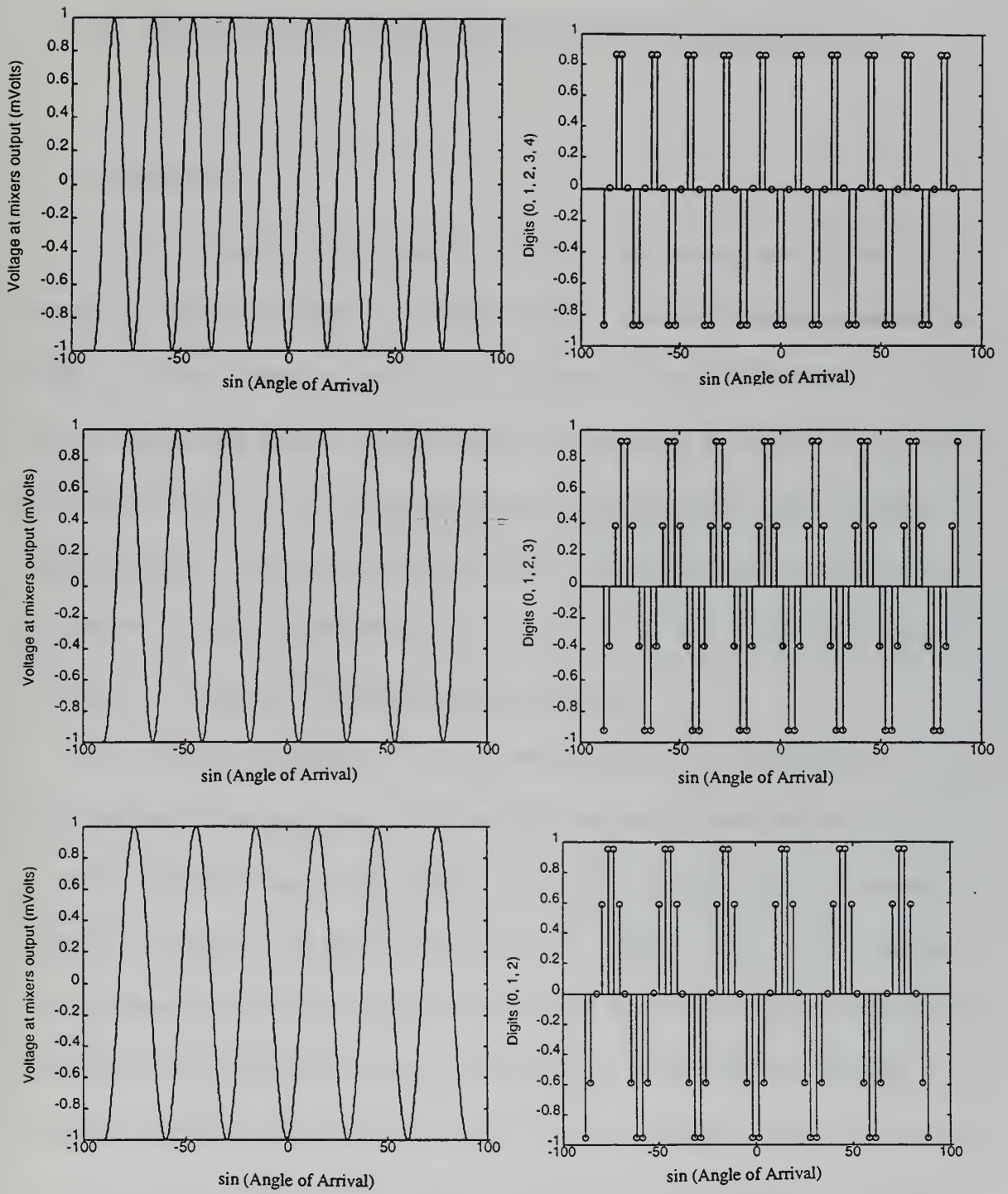
Figure 2.11: Plots before and after the quantization for the cases of (a) 3 digits / 5 λ baseline, (b) 4 digits / 3.75 λ baseline, and (c) 5 digits / 3 λ baseline.

31

III. PROTOTYPE ARRAY DESIGN AND FABRICATION

A. OVERVIEW

The block diagram of the prototype DF array beamforming network and signal processor is presented in Figure 3.1. It consists of three separate two-element arrays that sample the incident wavefront and mix the signals from the two branches. In this particular design there are four antenna elements. Element one is referred to as primary and is shared by all pairs. The other three elements are spaced at non integer multiples of a half wavelength. The distances are determined by the SNS that will be used to encode the angle data. In this case the moduli $m_1 = 3$, $m_2 = 4$, and $m_3 = 5$ are used because of the availability of existing SNS digital processing hardware.

Each channel, in addition to the two antenna elements, also contains two low noise amplifiers (LNAs) and a mixer. The amplifiers are used to boost the incident signal up to the operational range of the mixers. The mixer multiplies the two inputs, as described by Equation (2.9) and low-pass filters the output so that only the baseband phase component is present at the output. This voltage, whose level is proportional to the phase difference between the two inputs, is then passed to the SNS digital processor. The SNS digital processor first amplitude analyzes the phase response within each channel and then recombines these results in a logic block that produces the DOA, as described in the Section C of Chapter II.
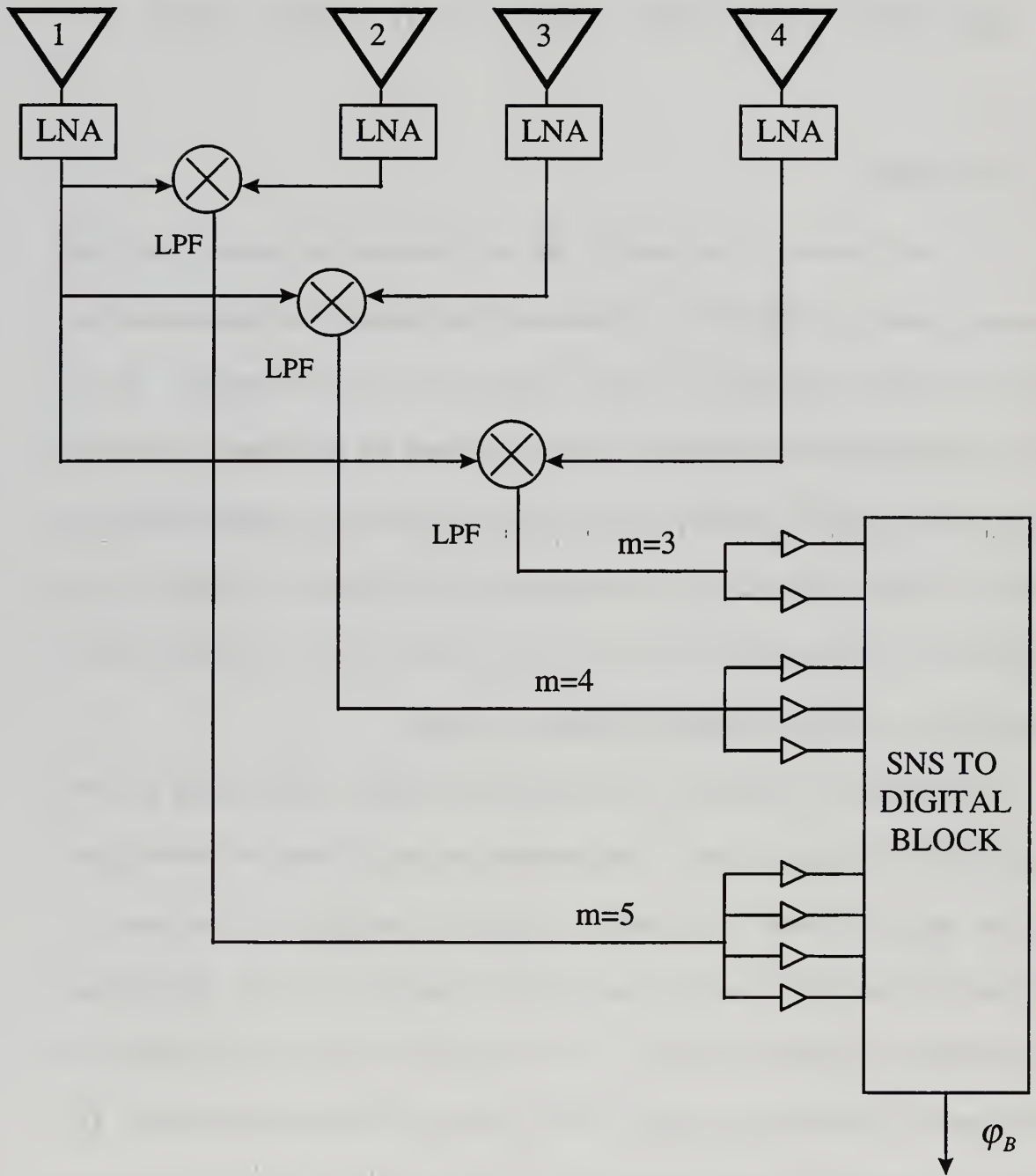
Figure 3.1: Block diagram of the prototype direction finding array.

The objective of this thesis is to design and construct a three array SNS DF antenna and verify its performance at 8.5 GHz by taking pattern measurements in the anechoic chamber. As a first step, the performance of the individual antenna components

are determined. The analysis has assumed ideal device characteristics, and any deviation from the non-ideal case must be compensated for in the design and assembly of the antenna. The performance of each component is determined using a network analyzer. The quantities of interest are the scattering parameters, or equivalently the reflection and transmission coefficients at both device ports. For the mixers, we are interested in the phase difference versus output voltage, while for the LNAs it is the input power versus output power relationship. Note that the knowledge of the phase is necessary for correct assembly of the beamformer.

An important step is the calculation of the appropriate length of the coaxial cables, and their fabrication. They must be adjusted to avoid any unwanted phase differences between the antenna elements and the mixer. The cable lengths are also used to shift the output phase response curves so that a minimum value occurs at $\varphi_B = -90^\circ$ for all channels. When constructed in the lab the cables insertion phase may only be within $\pm 5^\circ$ of the required phases. The remaining error is corrected by using adjustable phase shifters. Next, each channel gets assembled and tested in the lab under similar conditions to those expected in the chamber. That is, pairs of elements are excited with equal amplitude phase-shifted waves to simulate an incident plane wave. Finally, data is collected in the anechoic chamber.

B. MIXER DATA

In Chapter II we presented the operation of a mixer and we derived the formula that relates its output voltage to the phase difference of its inputs:

$$v_{out}(t) = \frac{V^2}{2} \cdot \cos(\Delta\alpha) \qquad\qquad (3.1)$$

This is the ideal result; an actual mixer will deviate from this. Furthermore the mixers are not identical, i.e., there will be variations in the DC output level for similar signals at their inputs. It is necessary to test the individual mixers and record the differences in performance so that they may be accounted for in the design. The approach is to create a signal of 8.5 GHz and send phase shifted versions of it through cables to both inputs of the mixers. Phase differences were obtained with phase shifters in one branch, thus simulating a plane wave excitation at the mixer input. The test setup includes a network analyzer with its signal generator, a power splitter, two phase shifters, and a voltmeter as shown in Figure 3.2.

Semi-rigid coaxial cables were used to make connections to the mixers so that phase stability could be maintained. Since these cables are not flexible, they have to be constructed and laid out in such a way as to fit between the radiating elements and mixers. The vector network analyzer generated a signal of 15 dBm. Although this signal is less than that expected in the chamber, it was the maximum possible from the analyzer. The signal was passed through a power splitter yielding two identical signals at half of the incident power. Each signal was sent to a mixer input. The branches included phase shifters to introduce a phase shift. One branch included a 10 dB directional coupler to serve as a reference. The -10 dB output of the coupler was connected to the network

analyzer. The circuit also included several different adapters and barrels to interconnect different types of cables and components.

Voltage measurements were taken from a voltmeter connected at the output of the mixer. Phase measurements should normally be measured directly at the input of the mixer. Unfortunately there was no way to measure the phase at these points without disconnecting the mixer every time. This is not only tedious and time consuming, but also reduces the accuracy of the phase measurements. Connecting and disconnecting components, moving or slightly bending cables, and connector torque can cause

Figure 3.2: Mixer output test configuration.

variations in phase shift. Phase measurements were taken from the vector network analyzer between the input of the power splitter and the -10 dB output of the coupler. To be precise they were taken between the 3.5-female-to-N-male adapter and the male-to-male-barrel. The presence of these components cause a phase shift which also has to be taken into account. Figure 3.2 shows the test points of the measurements.

A reference phase was obtained by measuring the phase difference between points A and B of Figure 3.2, and their respective mixer inputs C, D and then subtracting it out to get the desired phase difference. The phase reference point was chosen as the input of the 3.5-female-to-N-Male adapter where the first port of the vector network analyzer was connected (A). The phase difference between this point and the output of the phase shifter at the first branch (C) was found to be -57.1 degrees. For the second branch the output of the male-to-male-barrel after the -10 dB output of the coupler (B) had a phase difference of -168.3 degrees, while at the barrel before the mixer at point D (with the -10 dB output of the coupler matched) was 150.4 degrees. The measured and computed phase differences (in degrees) are:

$AB = -57.1$

$AD = 150.4$

$AC = 168.63$

$BD = AD - AB = 150.4 - (-57.1) = 207.5$

$CD = AD - AC = AB + BD - AC = AB + 207.5 - 168.63 = AB + 38.87$

For every phase measurement taken it was necessary to add 38.87 degrees to refer it to the phase difference at the input of the mixer.

Phase shifters were used to change the phase, which was recorded at the network analyzer, and the output voltage at the voltmeter. The results are presented at Table A.1 in Appendix A, and a plot shown in Figure 3.3. The gray line shows the theoretical result. The comparison of the two shows that the general behavior of the mixer was as expected. The differences are within the measurement accuracy of the test set-up.
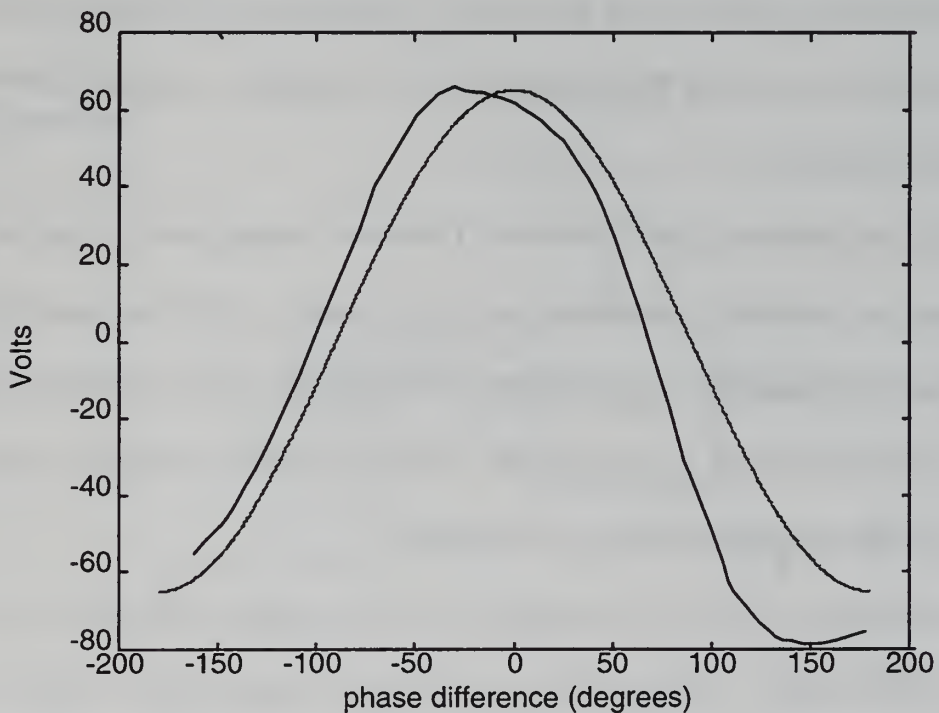
Figure 3.3: Comparison of the actual response of the mixer with the theoretical.

C. LOW NOISE AMPLIFIER DATA

Low noise amplifiers (LNAs) are used in radar and direction finding systems to increase signal level without introducing significant noise. Therefore, they not only increase the signal power level, but also to improve the signal-to-noise ratio (SNR).

The antenna receives both signal and noise. Also every component in the receive channel contributes thermal noise, which adds to the total noise. Components like mixers have a high noise figure F, where $F = \dfrac{SNR_{in}}{SNR_{out}}$. LNAs on the other hand introduce little noise, yet amplify the signal such that the SNR is increased. The noise introduced by a mixer can be several times the noise of the LNA, but because the SNR was increased by the LNA its effect on the total signal-to-noise ratio is negligible. A typical noise figure for an LNA is around 1dB.

LNAs can introduce signal distortions. The power input to power output response is not linear and eventually the output power will saturate. Also, the phase shift vs frequency can be different for every individual LNA depending on its construction, which cannot be predicted and has to be measured. The linear and the saturation ranges are important to know for proper operation of the antenna.

In the array, the low noise amplifiers are to be connected between the antenna elements and the mixers. The amplifiers will be operated in the saturation region so that the output power level remains constant for the expected variation in input level. According to Equation (3.1) the voltage level at the output of the mixer depends not only on the phase difference but also on the maximum voltage level of the mixer's input signals. If the amplifiers were not included, the maximum voltage level would drop off

with angle from boresight due to the element factor. The output of the mixer would be dependent on the signal strength, and the DC signal would not be a constant amplitude sinusoid. Sources at different angles, would create different voltage levels at the mixer output, even if they were at the same range. Operating the LNAs in the saturation region alleviates this problem. The LNAs were manufactured to be phase matched within 10 degrees.

To determine the operating characteristics of the LNAs, a signal generator and two power meters were used as shown in Figure 3.4. The signal generator was connected
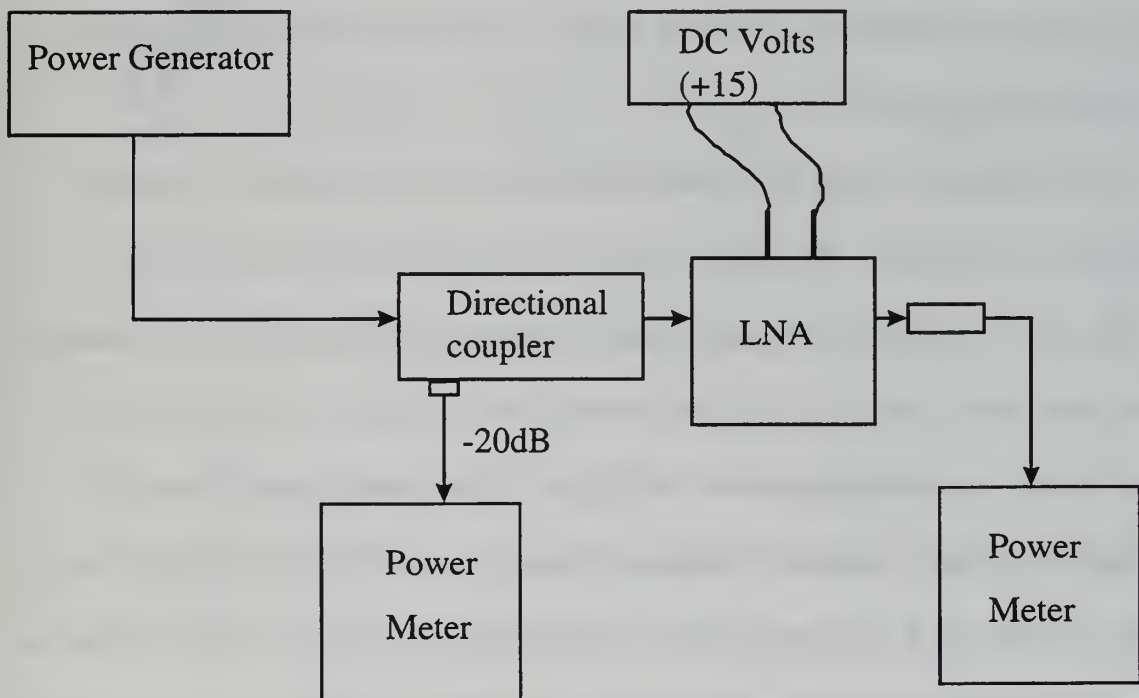
Figure 3.4: Input vs output power measurements for the LNAs.

to a - 20 dB directional coupler. A power meter connected at the -20 dB output was used measure the input power level. The LNA was connected to the through port of the coupler and the second power meter was connected to the output of LNA to measure the output power level. A DC voltage source of 15 volts was connected to the LNA to activate it. Also a heat sink was attached to the LNA to ensure that heat damage would not occur. At this point phase was not measured, first because the LNAs were ordered to be phased matched, and secondly, the phase difference of the entire branch will be measured before final assembly. For these measurements the input power level was increased and the output power level recorded. A problem that we faced was that the output did not settle down immediately, but there were some fluctuations and it was necessary to wait considerably to get a stable reading. This in turn increased the problem of overheating of the LNAs.

The determination of the input power range used for the measurements was based on the hardware limitations. The signal generator had a maximum power output of - 9 dBm. Thus this value determined the maximum signal power value used. On the other hand the power meter input had a minimum sensitivity of - 60 dBm. Since the signal to the power meter was passing through the - 20 dB arm of the coupler, the minimum value of the signal before the coupler that would be detected was - 40 dBm. This input power range of - 40 dBm to - 9 dBm was adequate for our purposes. Because of the coupler, every measurement value taken from the power meter had to have 20 dB.
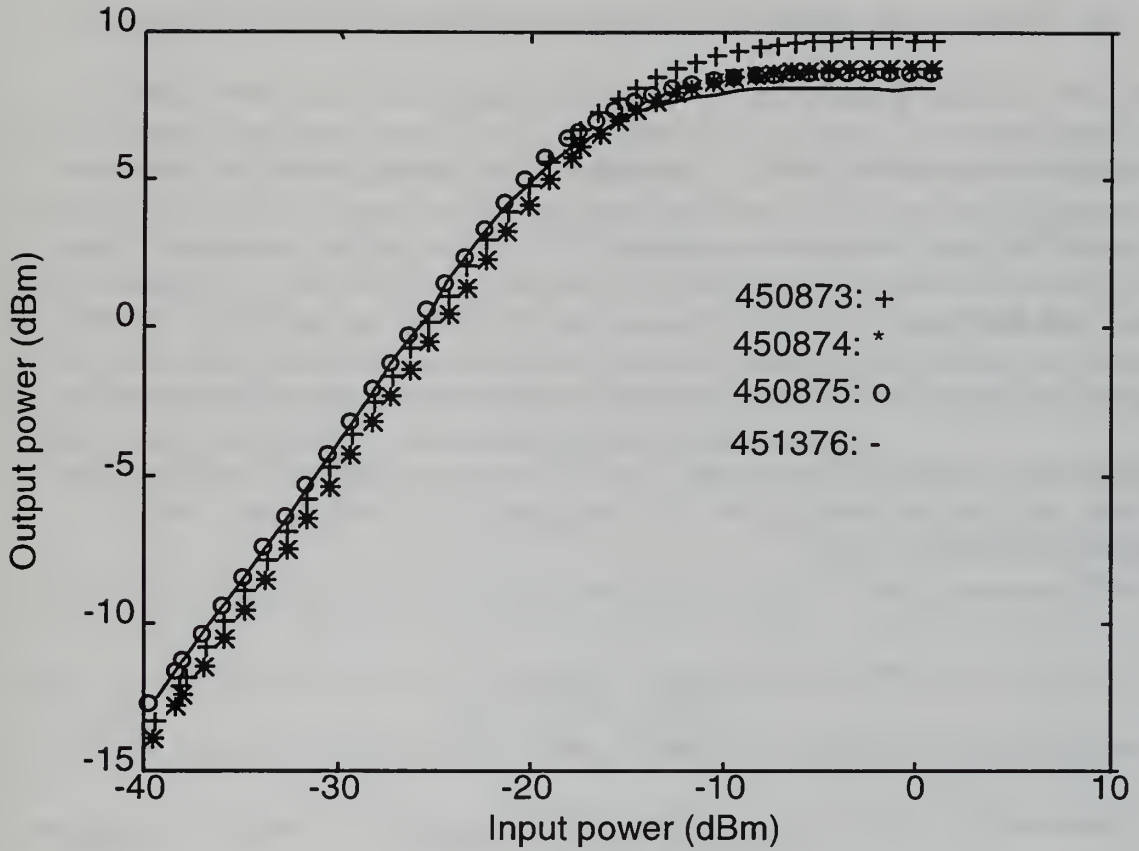
Figure 3.5: Plot of input vs output power for the four LNAs.

Figure 3.5 present the plots of input power versus output power for the four LNAs. Tables B.1 through B.4 in Appendix B present the raw data. From Figure 3.5 we can see that the curves are matched and initially linear up to about - 28 dBm input power. After -20 dBm they saturate. There are some minor differences in the curves between the amplifiers, although these differences are not expected to influence the DF performance.

D. DESIGN OF THE ARRAY

The first task in the design of the array is to calculate the distance between the element pairs. An array ground plane had already been fabricated for an array based on a residue number system (RNS) [Ref 5]. Although the RNS spacings are not the same with those for the SNS array, the existing spacings of 10λ, 7.5λ, and 6λ were used. These are twice what they should be for an SNS array. An SNS-to-decimal-logic-block for three channels of two, three, and four reference levels for digitization were used because of the availability of an existing A/D converter. For SNS arrays, the number of periods within 180 degrees are (Equation 2.13)

$$n_1 = \frac{2d_1}{\lambda} = \frac{2 \cdot 10\lambda}{\lambda} = 20 \qquad (3.2a)$$

$$n_2 = \frac{2d_2}{\lambda} = \frac{2 \cdot 7.5\lambda}{\lambda} = 15 \qquad (3.2b)$$

$$n_3 = \frac{2d_3}{\lambda} = \frac{2 \cdot 6\lambda}{\lambda} = 12 \qquad (3.2c)$$

while Equation (2.15) determines how many periods can be covered unambiguously

$$n_1 = \frac{M}{2m_1} = \frac{60}{2 \cdot 3} = 10 \qquad (3.3a)$$

$$n_2 = \frac{M}{2m_2} = \frac{60}{2 \cdot 4} = 7.5 \qquad (3.3b)$$

$$n_3 = \frac{M}{2m_3} = \frac{60}{2 \cdot 5} = 6 \qquad\qquad (3.3c)$$

Since the element spacings are twice what they should be for an SNS array, unambiguous angle estimates will not be possible with the prototype design over the entire 180 degrees. In fact, depending on which angles are chosen, the unambiguous interval can be from 60 to 90 degrees. This restricted sector for unambiguously determing the DOA is sufficient to demonstrate the feasibility of the concept and detail its advantages.

Another issue needed to be taken care of is the alignment of the three array voltage outputs so that they have a minimum value at $\varphi_B = -90°$. The importance of this is shown in Table 2.2, where we can see that the digits must start from the values (0, 0, 0). We can control the location of the voltage minima by introducing the appropriate phase shift to the signals at a point between the elements and the mixer. The normalized output voltage of the mixer is given by Equations (2.11) and (2.7):

$$v_{out} = \cos[2\pi \cdot \frac{d}{\lambda} \cdot \sin(\varphi_B) + \psi_0]$$

For a minimum value, $v_{out} = -1$ at $\varphi_B = -\frac{\pi}{2}$ requires that

$$(2k + 1)\pi = -2\pi \frac{d}{\lambda} + \psi_0 \ , \qquad k = 0, \ \pm 1, \ \pm 2,...$$

or

45

$$\psi_0 = (2k + 1 + 2\frac{d}{\lambda})\pi \qquad\qquad (3.4)$$

For each array spacing d Equation (3.4) can be used to determine the appropriate phase shift necessary to shift a minimum to $\varphi_B = -90°$

$$d = 10\lambda, \Rightarrow \psi_{01} = \pi$$

$$d = 7.5\lambda, \Rightarrow \psi_{02} = 0$$

$$d = 6\lambda, \Rightarrow \psi_{03} = \pi$$

The phase shift calculated above is introduced by adjusting the cable lengths. The construction of the cables is very important in the development of the direction finder which uses the phase delay method to determine DOA. Since direction is calculated from phase difference, variations in phase from the ideal introduce AOA errors. Cable length is a critical parameter especially for signals at 8.5 GHz, where the wavelength is 3.53 cm, and thus phase changes 360 degrees within this distance. Thus a moderate error in the length can affect the AOA estimate significantly. Other factors also introduce phase shifts: bends in the cable, loose connections, adapters, and transitions. All of the phase variations between the array channels must be measured. Once they are known they can be compensated for by adjusting the cable lengths.

E. CONSTRUCTION OF THE FIRST CHANNEL

To describe the construction process we consider the array with the baseline of 7.5 λ. It consists of the two branches, each with one antenna element, connected to a mixer. As detailed in Section C, the signal after the antenna elements had to be amplified to a standard level with the use of LNAs. It was clear that the LNA must operate at the saturation level in order to provide a constant amplitude sinusoidal shaped output. The incident signal was expected to be around - 40 dBm. But from Figure 3.5, with this input, the output of an LNA is only around - 6 dBm and operates in the linear range. Therefore, when operating in the anechoic chamber the amplifier outputs, and hence the mixer outputs, will not be constant under all conditions as required to Equation (3.1). The problem can be avoided by using two LNAs in series. The input to the second one, at - 6 dBm, gives an output around + 9 dBm, which is in the saturation region of the second LNA. Thus two LNAs are used for every branch. Since there were only four LNAs available, it was only possible to have only one channel operational at any given time.

The individual components in the two branches were connected together with the semi-rigid cable. Cables of approximately the same length were used and additionally phase shifters were added to trim any residual phase difference. The trimming of the phase was performed with the help of the vector network analyzer. The phase differences between the two ends of the branches were measured and the phase shifters adjusted until they were equal. The test diagram is shown in Figure 3.6. The branch whose phase shift is to be measured is located between the two arrows. Since the antenna element

VECTOR NETWORK ANALYZER

15 VOLTS DC

-8dB

-19dB

ADAPTER
x218c

ANTENNA

7mm to APC-7 ADAPTER

L
N
A

L
N
A

-4dB

PHASE SHIFTER ⟶
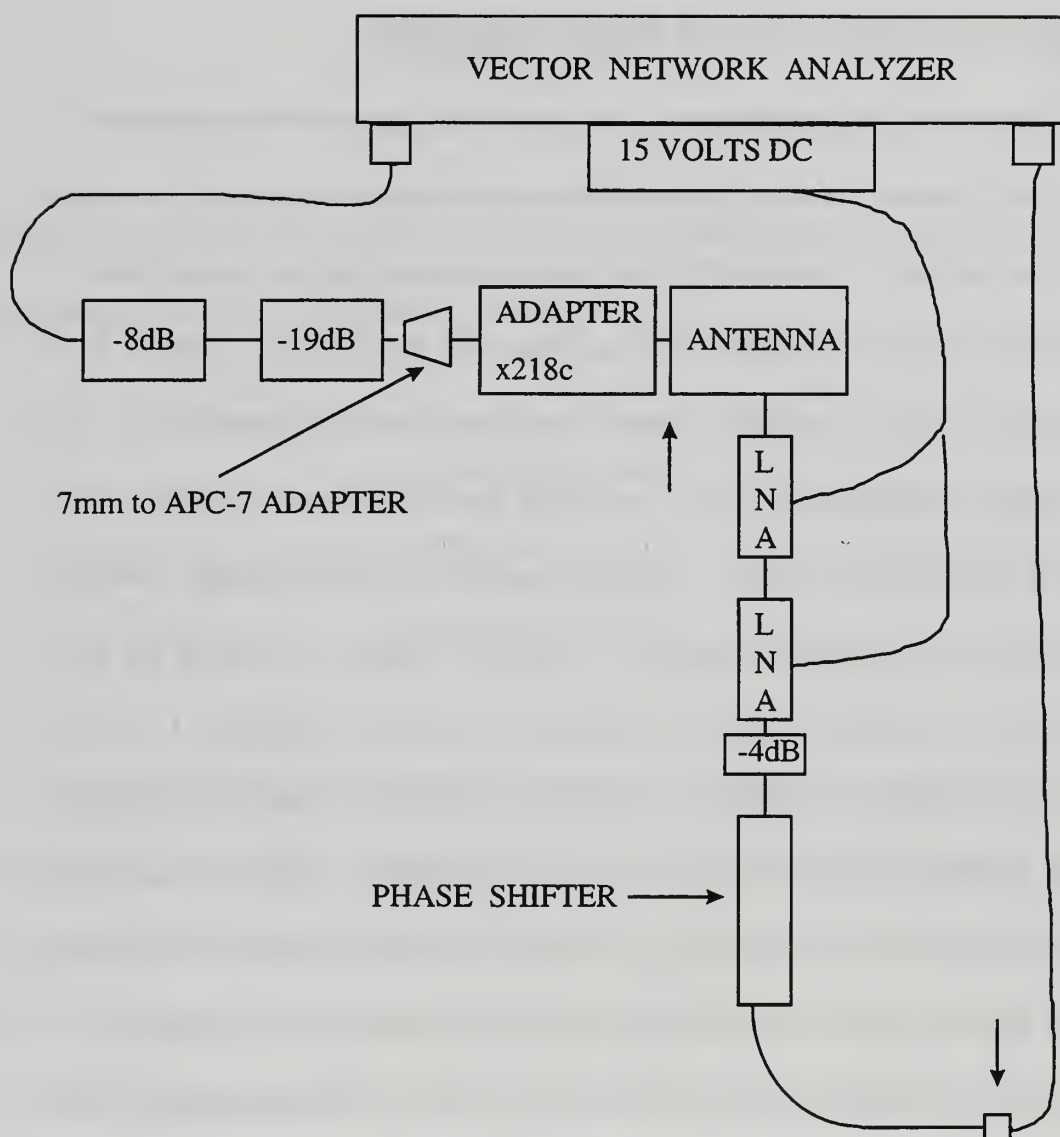
Figure 3.6: Test set up for phase difference measurements on a branch.

is on one end, it had to be disconnected and attached to the analyzer using adapters. This

introduces an additional phase but it is constant for all channels measured and therefore

will not contribute any error to the phase differences. The vector analyzer power output

is from -15 dBm to 15 dBm. Since we wanted a signal of - 40 dBm at the antenna, we

used an input power of -13 dBm and two attenuators of - 8 dB and - 19 dB. This lowers the power at the element to the desired level.

The phase difference found in the first branch was 117 degrees while for the second it was found to be 135 degrees. By adjusting the phase shifters both of them were set to 125.5 degrees. After adjustment, the phase shifters were "locked" and the channel assembly was completed. Figure 3.7 presents a picture of the beamforming circuitry for the first array.
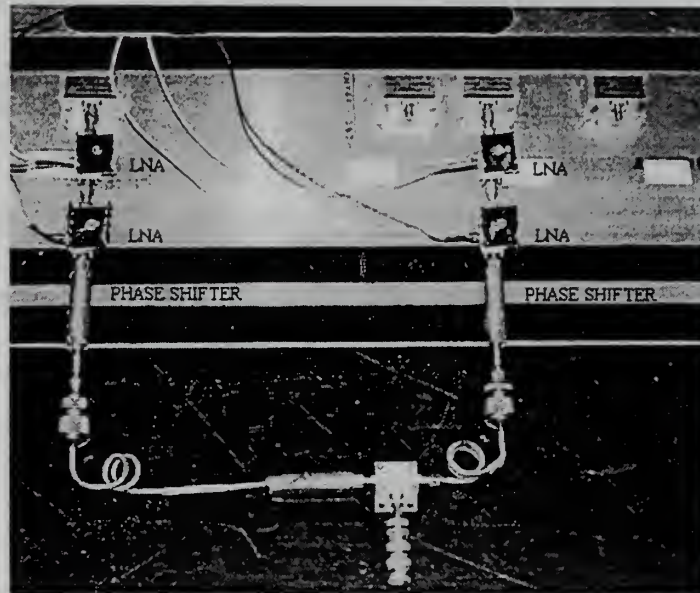
Figure 3.7: Constructed channel, $d = 7.5\lambda$.

F. CHECK OUT OF THE FIRST CHANNEL

After the assembly of each channel, its operation was verified in the lab by exciting the elements under similar conditions with those expected in the anechoic chamber. The objective of this test was to verify that the output of the mixer was proportional to the phase change, and that the change was sinusoidal-like. This was accomplished using the network shown in Figure 3.8. With the use of adapters the two antenna elements were connected to the analyzer signal source. Attenuators were inserted to drop the power level at each antenna element to -40 dBm. One of the branches had a phase shifter to create a phase difference, which simulates an off broadside incidence angle. Thus we produced conditions very similar to the ones at the chamber. A voltmeter connected at the output of the mixer measured the DC voltage.

The measurements verified the predicted performance. The DC voltage level changed in a sinusoidal-like fashion between -295 mV to 290 mV (approximately). Also, the procedure showed that the heat sinks on the LNAs were working properly, even for an extended period of on time. This was very important, since in the chamber we do not have immediate access to the board should a component have to be removed.
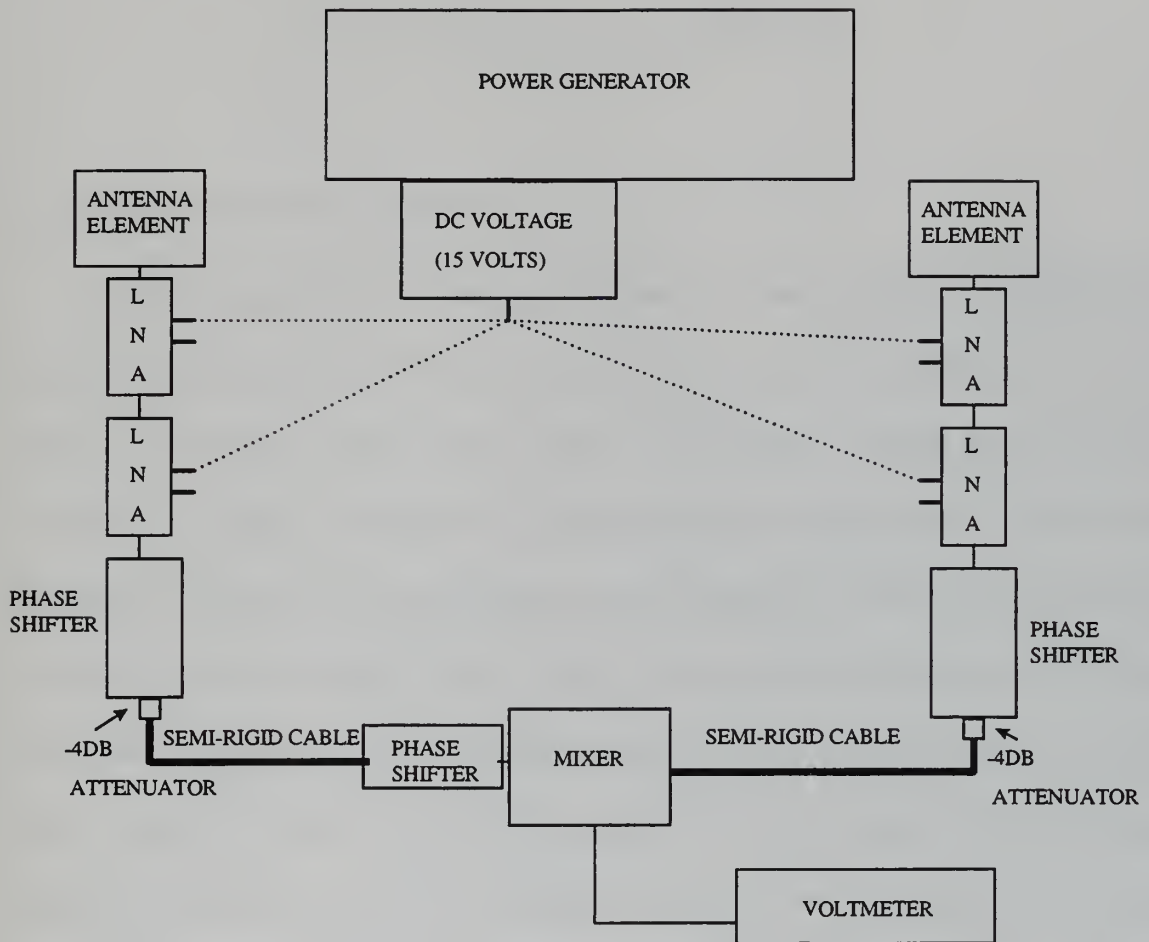
Figure 3.8: Test of the first channel at the lab.

IV. EXPERIMENTAL RESULTS

A. EXPERIMENTAL SET-UP

Chapter III described the design of the direction finder and the tests performed to ensure its proper operation. After completing all these steps the two element system was taken to the anechoic chamber for the pattern measurements. Special mounts for the LNA DC voltage supply connectors had to be constructed, so they would not loosen up or get disconnected while the antenna rotates inside the chamber. In the chamber there was one DC bias connector of BNC type to which all the cables were connected. The LNA cables had one bare end which was soldered to the LNAs and then covered with dielectric rubber. Figure 4.1 shows an LNA with its heat sink and its permanent DC voltage connections. The darker (red) one is the positive lead while the white one is the ground. The other ends had banana plugs and were connected to an appropriate adapter to a BNC connector. Finally, the beamforming circuit and the two elements were mounted on the ground plane containing the radiating elements. For the first test the spacing between the elements was 7.5 wavelengths. Figure 4.2 shows an element mounted on the back side of the ground plane. Figure 4.3 shows the front side of a ground plane. The element shared by all of the arrays is on the far right and the spacings from right to left are 6, 7.5, and 10 wavelengths, respectively.
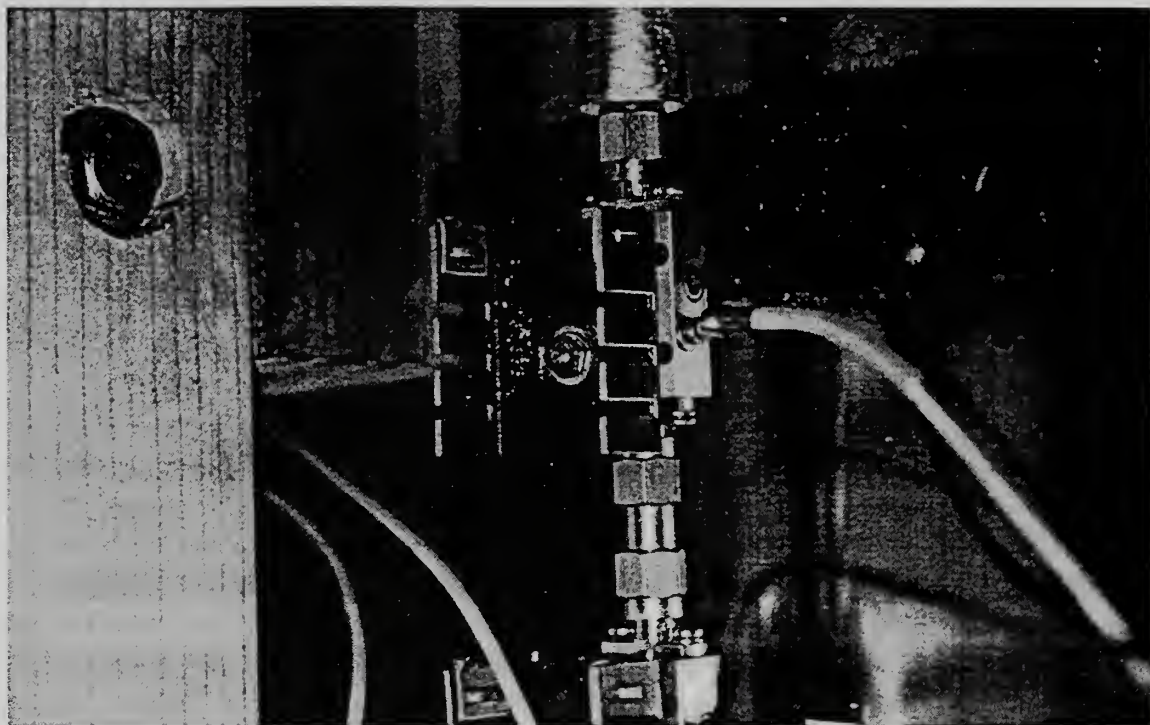
Figure 4.1: LNA with a heat sink connected at the system.
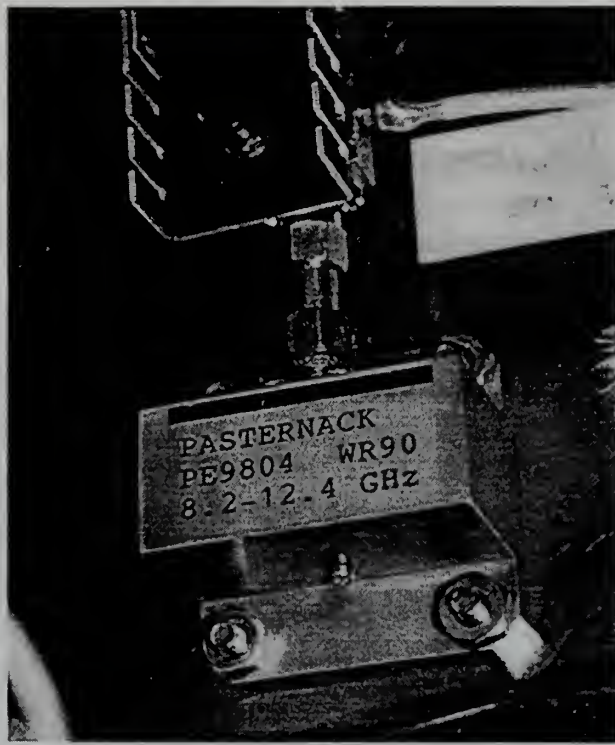
Figure 4.2: Antenna element mounted at the back aside of the ground plane.

Figure 4.3: Front side of the ground plane.

In the chamber there is a transmitting source which is fixed on the wall facing the pedestal where the receiving antenna is mounted. Both the transmit and receive antenna are at the same height, so the elevation angle of arrival is $\theta = 90^o$. The base rotates from -90 degrees to 90 degrees with 0 degrees being broadside to the array axis. Thus sources located in all directions within the interval $-\frac{\pi}{2} \leq \varphi_B \leq \frac{\pi}{2}$ can be simulated. The transmitter, receiver, and pedestal are all computer controlled. Figure 4.4 shows a picture of the transmit antenna, and Figures 4.5 and 4.6 show the mounted receiving antenna base.
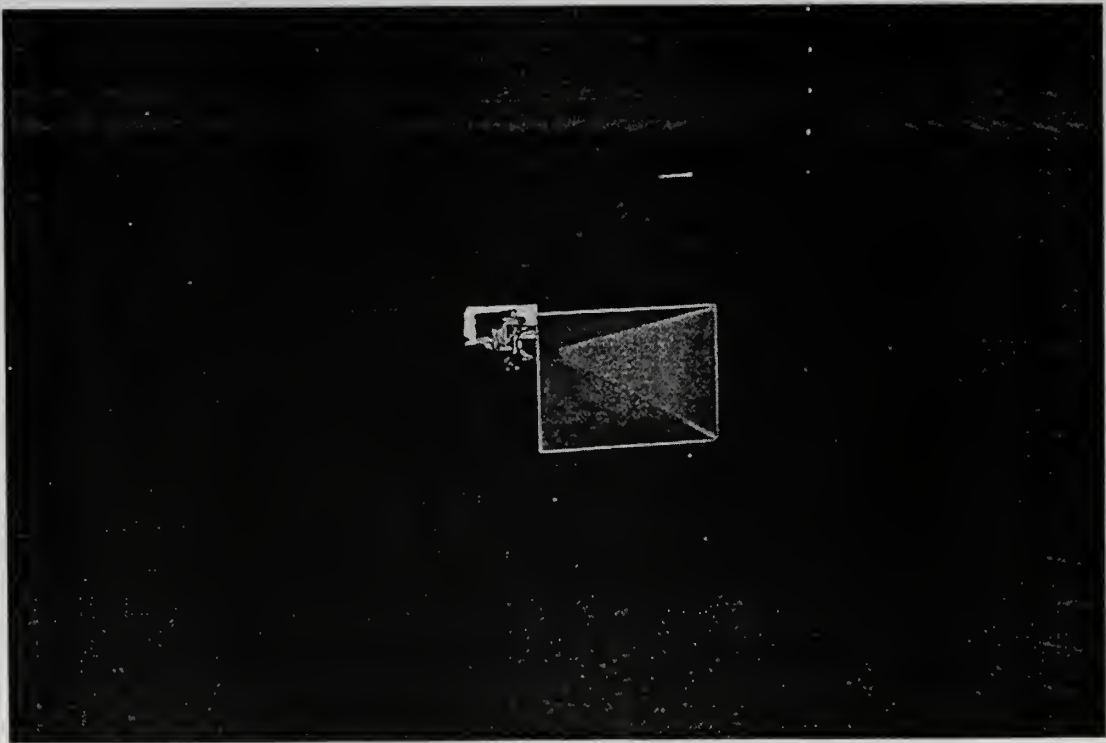
Figure 4.4: Transmitting antenna in the anechoic chamber.
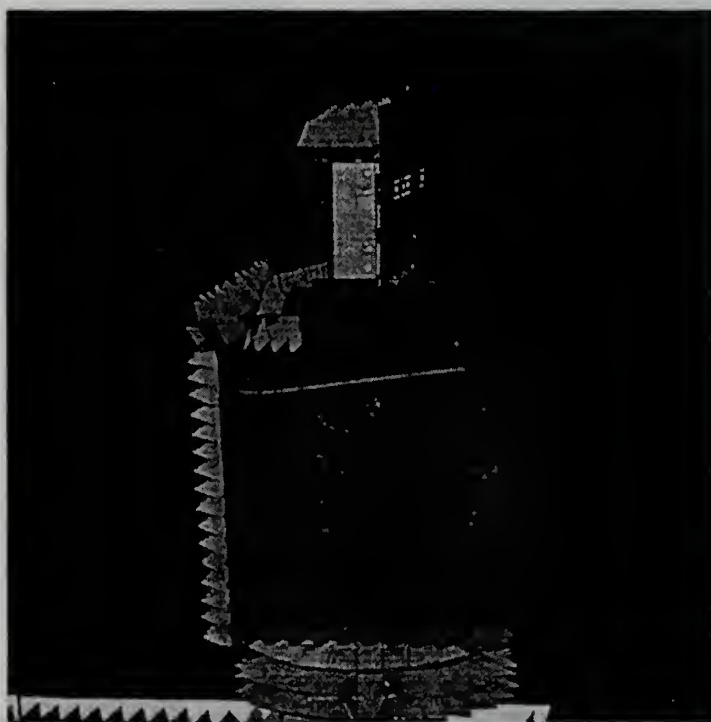
Figure 4.5: Receiving antenna and pedestal (side view).
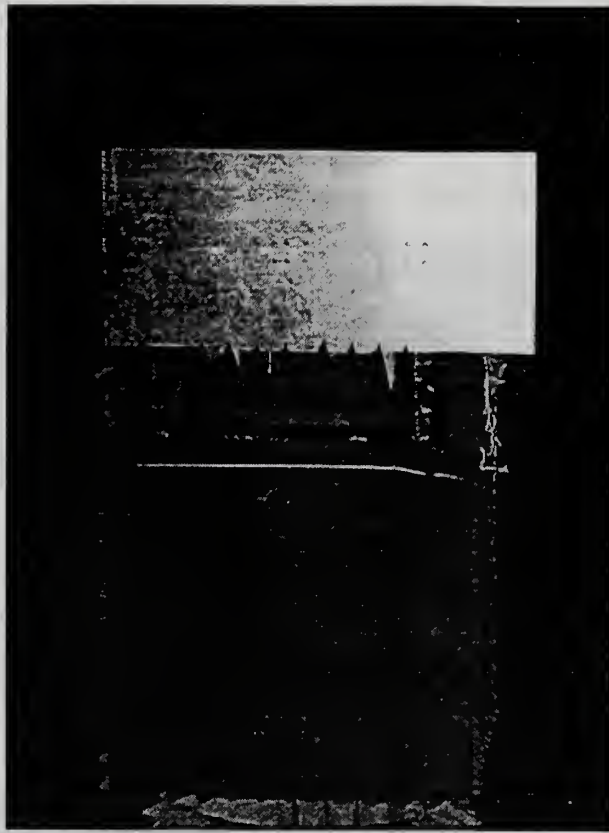
Figure 4.6: Receiving antenna and pedestal (front view).

The board was mounted at the base using Velcro bands. They provide stability yet are flexible for adjustments and permit the board to be easily removed and replaced. The cables for the LNAs were connected to the DC source, and the output of the mixer with the voltmeter. Except for the front side of the ground plane (receiving antenna) everything was covered with anechoic material to absorb the spurious waves and avoid reflections. The antenna was accurately aligned so that angle errors were negligible. Alignment was accomplished using a laser pointer with a narrow beam. By placing the laser beam perpendicular to the ground plane above the center of rotation, it was possible

to place the laser beam on the transmit horn thereby aligning the test antenna to the emitter.

Located in the adjacent instrumentation room are the voltmeter, the voltage source which provides the 15 Volts DC to the LNAs, the HP8510 network analyzer, and the computer controller. The latter is used to control the transmitter signal and the rotation of the pedestal. It was programmed to sample the voltmeter and record the measured DC values out of the mixer at specified angles. The data were taken manually by two people. The first person called out the angle and the second recorded the DC voltage at that instant. The measurements were taken every 0.5 degrees from - 90 to 90 degrees. For each channel the measurements were taken several times so that any measurement errors could be uncovered. However, all data repeated without any significant deviations.

B. MEASURED ARRAY RESPONSE DATA

The measurements on the first channel were taken and the ideal response vs measured response is shown in Figure 4.7. The gray line presents the ideal and the black the measured data. The differences are very small for angles between -60 and 60 degrees. Outside this region the errors are larger due to the reflection and scattering from the edges of the ground plane which are illuminated by the source at these angles. Another source of difference is the element patterns of the open-ended waveguides. Near $\varphi_B = 0^o$ the element patterns vary little but towards $\pm 90^o$ mutual coupling differences are significant due to the nonperiodic spacing of the elements.
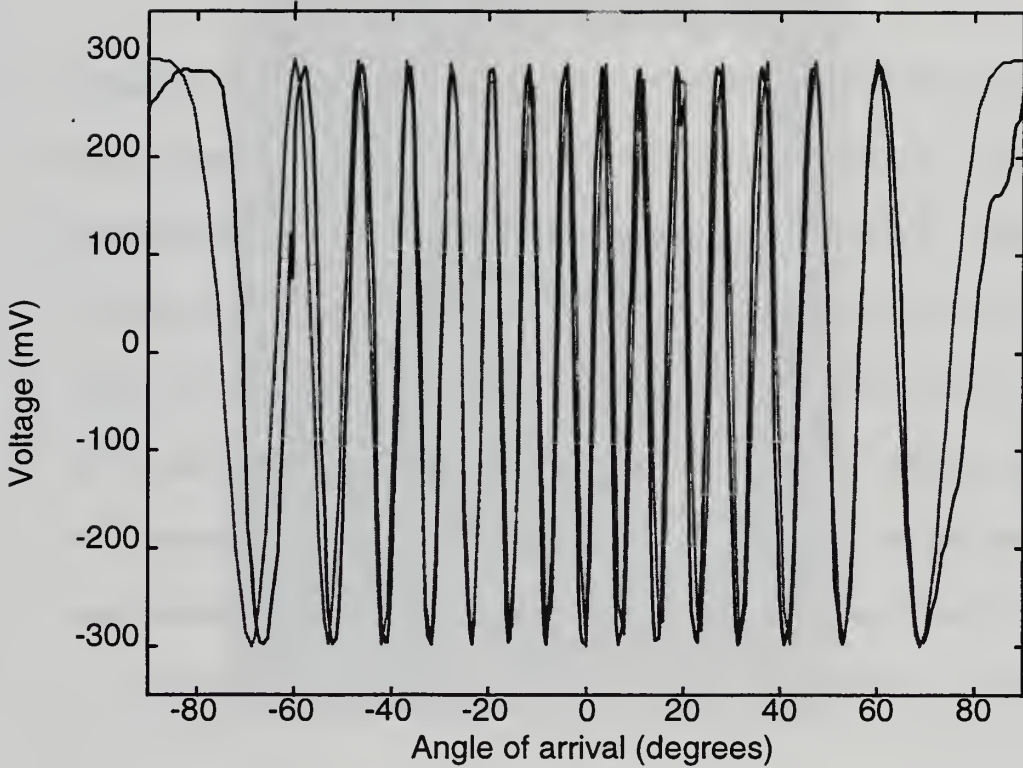
Figure 4.7: Plot of ideal vs measured data for $d = 7.5\lambda$.

The measurements of voltage mixer output versus angle of incidence as they were taken from the computer and the voltmeter are presented in Appendix C (Tables C.1 to C.4).

Response data was measured for the second channel whose baseline was 0.6 wavelengths. The construction procedure was similar to that for the first channel. As mentioned, since we had only four LNAs, the first channel had to be disassembled in order to construct the second. The measurements were taken using the same procedure as described for the first channel. Figure 4.8 shows the ideal (gray curve) and the measured

data (black curve) for the voltage at the mixer output versus angle of incidence. Within the area of interest (-60 to 60 degrees) the only deviation observed is a phase shift (i.e., translation of the curve along the horizontal axis). For this signal to be of use in the SNS logic block, the voltage must have its minimum value at -90 degrees. Although the channel was designed to add the appropriate ψ_0 an unwanted phase shift occurred during assembly, leading to a shifted curve. Additional phase trimming can eliminate this mismatch. Tables C.5 to C.8 in Appendix C present the measurements of voltage mixer output versus angle of incidence as they were taken from the computer and the voltmeter.
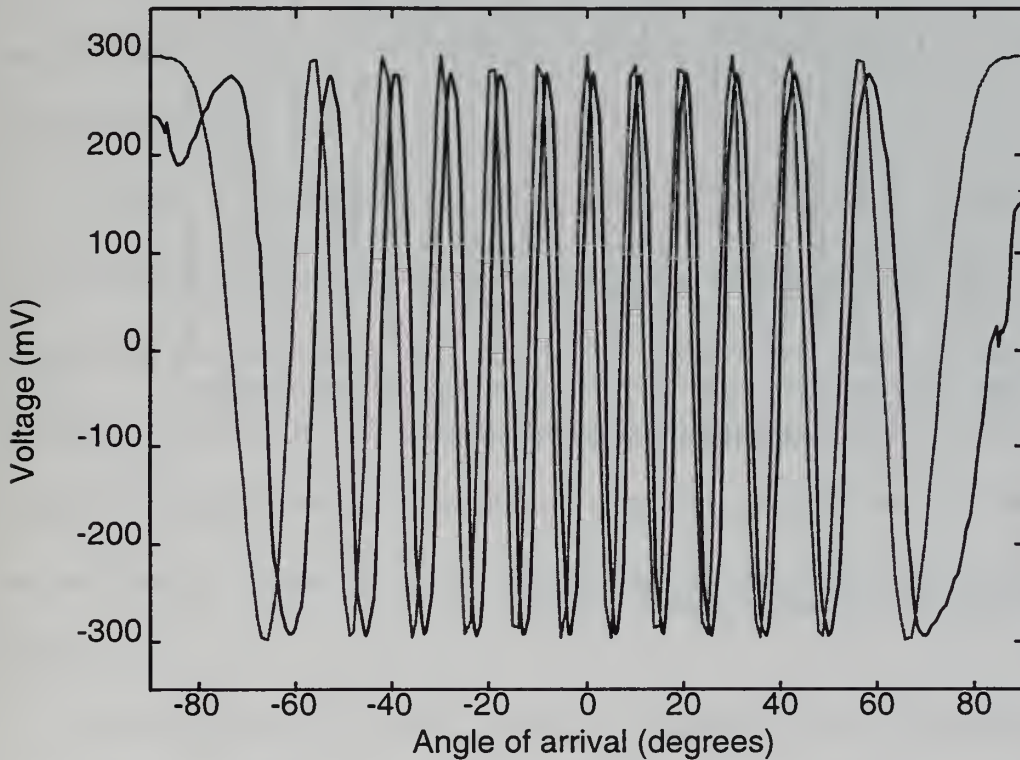
Figure 4.8: Plot of ideal vs measured data for $d = 6\lambda$.

The third channel's ideal (gray curve) vs measured (black curve) data plot is presented in Figure 4.9. Again a phase shift is observed for the same reasons as before. Tables C.9 to C.12 in Appendix C present the measurements of voltage mixer output versus angle of incidence as they were taken from the computer and the voltmeter.
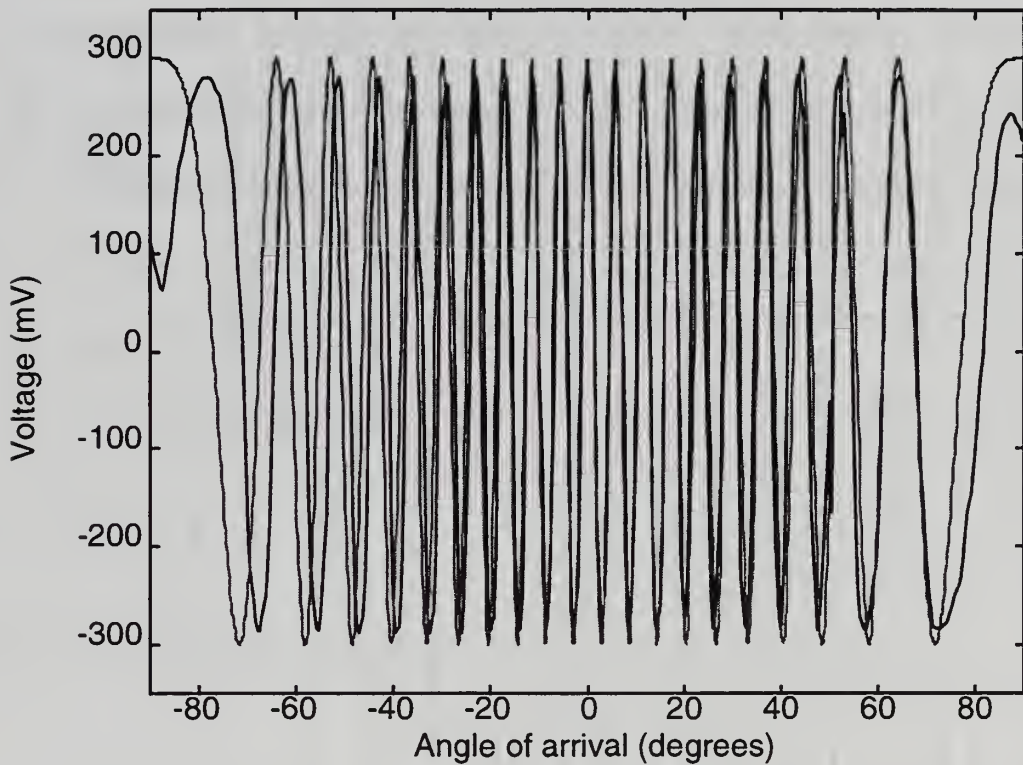
Figure 4.9: Plot of ideal vs measured data for $d = 10\lambda$.

V. CONCLUSIONS

This thesis discussed the design and construction of a direction finder which uses the phase comparison method to determine the direction of the emitter. The frequency of interest is 8.5 GHz and the processing of the signal is performed with a logic block whose operation is based on the symmetrical number system. Four antenna elements are used forming three pairs, with one element common for all the pairs. The output of the two elements of each pair are mixed together, and the DC voltage at the output is fed the logic block. In the course of this research all the components were tested and the arrays assembled and measured in the anechoic chamber to verify that their operation was as expected from theory.

The use of an already fabricated and available ground plane for an array based on a residue number system limited the angular range of unambiguous angle estimates compared to the larger range that would exist had the array been designed for SNS processing. Also the lack of some hardware components such as LNAs restricted the scope of the research: only one channel could be constructed and tested at a time. Thus it was not possible to test the whole array and beamforming network in the anechoic chamber.

The measured results were in agreement with theory. The curves had the same number of cycles as predicted by the equations, but were phase shifted (translated) because of phase deviations unintentionally introduced in the assembly process. For the curves to be usable for the SNS logic block, they must have a minimum voltage value at - 90 degrees, which was not true for two arrays due to the unintended phase shifts. A

further phase trimming on the assembled antenna can easily eliminate the unwanted phase differences. The SNS direction finding array has great promise for providing accurate, unambiguous DOA estimates and this research has provided a proof of concept.

The next step should be the assembly of the entire array and beamforming network. To accomplish this more amplifiers must be purchased. The three channels can then be tested as a direction finding array by connecting the DC output to the SNS A/D converter.

After the array performance has been demonstrated a new aperture should be constructed with the proper SNS element spacings, which are 3, 3.75, and 5 wavelengths respectively. Using these distances between elements unambiguous DOA estimates can be obtained.

Future studies should also examine the quantization error characteristics and the frequency correction schemes proposed in [Ref 5].

APPENDIX A: MIXER DATA

Phase	Volts	Phase	Volts	Phase	Volts	Phase	Volts	Phase	Volts
177.5	-75.3	109	-62.4	45	34.9	-11.4	63.8	-117.8	-19.2
163	-77.7	106	-56.8	42	38.2	-16.3	64.7	-124	-26.3
155	-78.7	100	-49.2	37	42.5	-20	64.3	-130.3	-33.3
146	-78.8	89	-34.7	32	46.7	-25.7	65.1	-136	-37.6
140	-78.8	86	-31.1	25	51.7	-29.7	65.8	-142	-42.9
136	-77.7	79	-17.3	19	54.8	-37.9	64.2	-145.7	-45.6
133	-76.9	69	-0.3	14	57	-49	58.3	-148.5	-47.7
130	-75.5	64	7.6	9.2	58.7	-71	39.9	-157.5	-52.3
124.7	-72.8	59.9	14.3	3.7	60.2	-78	28.7	-162.5	-55
116	-67.8	52.3	25.6	0	61.5	-98	4.6		
111	-65.2	50	27.7	-7	62.9	-108.6	-8.6		

Table A.1: Measured voltage vs phase difference for the mixer.

APPENDIX B: LNA DATA

Input Power	Output Power	Input Power	Output Power	Input Power	Output Power
-59.4	-13.28	-45.32	0.16	-31.49	8.97
-58.2	-12.17	-44.33	1.07	-30.41	9.17
-57.8	-11.82	-43.32	2.05	-29.29	9.34
-56.8	-10.82	-42.28	2.97	-28.17	9.48
-55.8	-9.93	-41.22	3.89	-27.25	9.58
-54.78	-8.92	-40.14	4.77	-26.32	9.64
-53.7	-7.92	-39.05	5.62	-25.37	9.69
-52.6	-6.9	-37.99	6.38	-24.39	9.73
-51.55	-5.84	-37.47	6.7	-23.39	9.75
-50.45	-4.77	-36.53	7.27	-22.35	9.75
-49.31	-3.66	-35.56	7.72	-21.27	9.75
-48.16	-2.56	-34.58	8.09	-20.19	9.74
-47.24	-1.64	-33.57	8.43	-19.09	9.74
-46.29	-0.74	-32.54	8.74		

Table B.1: Input power measurements vs output power for LNA 450873. For the real input power values add 10 dB.

Input Power	Output Power	Input Power	Output Power	Input Power	Output Power
-59.5	-13.89	-45.33	-0.49	-31.7	8.09
-58.4	-12.77	-44.33	0.46	-30.6	8.28
-58	-12.44	-43.38	1.34	-29.46	8.44
-56.91	-11.5	-42.33	2.3	-28.32	8.55
-55.89	-10.55	-41.26	3.24	-27.41	8.64
-54.8	-9.55	-40.18	4.15	-26.48	8.71
-53.74	-8.56	-39.06	5.02	-25.56	8.7
-52.65	-7.52	-37.93	5.78	-24.56	8.74
-51.56	-6.47	-37.43	6.08	-23.55	8.76
-50.47	-5.42	-36.49	6.56	-22.51	8.76
-49.32	-4.31	-35.53	6.97	-21.42	8.75
-48.17	-3.21	-34.54	7.33	-20.33	8.74
-47.27	-2.34	-33.54	7.65	-19.23	8.72
-46.3	-1.42	-32.51	7.94		

Table B.2: Input power measurements vs output power for LNA 450874. For the real input power values add 10 dB.

Input Power	Output Power	Input Power	Output Power	Input Power	Output Power
-59.79	-12.76	-45.45	0.58	-31.67	8.24
-58.43	-11.63	-44.49	1.47	-30.59	8.36
-58.04	-11.29	-43.47	2.4	-29.47	8.45
-57.01	-10.36	-42.42	3.33	-28.35	8.52
-55.98	-9.42	-41.36	4.24	-27.44	8.57
-54.91	-8.45	-40.42	4.99	-26.51	8.59
-53.84	-7.44	-39.28	5.77	-25.56	8.6
-52.76	-6.41	-38.15	6.4	-24.59	8.61
-51.66	-5.35	-37.64	6.63	-23.58	8.6
-50.54	-4.28	-36.7	7.01	-22.54	8.59
-49.4	-3.18	-35.73	7.35	-21.46	8.59
-48.25	-2.08	-34.75	7.64	-20.37	8.59
-47.34	-1.21	-33.75	7.9	-19.26	8.61
-46.39	-0.3	-32.72	8.09		

Table B.3: Input power measurements vs output power for LNA 450875. For the real input power values add 10 dB.

Input Power	Output Power	Input Power	Output Power	Input Power	Output Power
-59.3	-12.52	-45.39	0.4	-31.47	7.81
-58.16	-11.42	-44.38	1.55	-30.39	7.91
-57.78	-11.1	-43.36	2.44	-29.28	8
-56.74	-10.19	-42.32	3.32	-28.15	8.06
-55.72	-9.26	-41.26	4.15	-27.24	8.1
-54.68	-8.33	-40.17	4.89	-26.31	8.11
-53.62	-7.34	-39.06	5.53	-25.35	8.11
-52.54	-6.33	-37.96	6.09	-24.38	8.1
-51.46	-5.31	-37.45	6.29	-23.38	8.08
-50.35	-4.25	-36.5	6.65	-22.34	8.06
-49.2	-3.15	-35.53	6.98	-21.25	8.05
-48.05	-2.07	-34.55	7.26	-20.17	8.06
-47.35	-1.25	-33.55	7.5	-19.08	8.07
-46.38	-0.38	-32.52	7.68		

Table B.4: Input power measurements vs output power for LNA 451376. For the real input power values add 10 dB.

APPENDIX C: MEASURED ARRAY RESPONSE DATA

Angle	Volts	Angle	Volts	Angle	Volts	Angle	Volts	Angle	Volts
-90	250	-80	289.4	-70	-117	-60	226	-50	-160
-89.5	255	-79.5	289.4	-69.5	-180	-59.5	257	-49.5	-74
-89	258	-79	289.3	-69	-220	-59	280	-49	33
-88.5	262	-78.5	289.1	-68.5	-254	-58.5	287	-48.5	129
-88	265	-78	288.7	-68	-274	-58	293	-48	207
-87.5	268	-77.5	287.9	-67.5	-288	-85.5	284	-47.5	257
-87	271	-77	286.4	-67	-296	-57	259	-47	285
-86.5	275	-76.5	284.2	-66.5	-298	-56.5	220	-46.5	294
-86	278	-76	280	-66	-294	-56	170	-46	285
-85.5	279	-75.5	274	-65.5	-293	-55.5	99	-45.5	260
-85	284	-75	273	-65	-272	-55	28	-45	215
-84.5	286	-74.5	255	-64.5	-253	-54.5	-75	-44.5	154
-84	289	-74	240	-64	-220	-54	-159	-44	67
-83.5	288	-73.5	215	-63.5	-204	-53.5	-230	-43.5	-36
-83	290	-73	190	-63	-140	-53	-265	-43	-155
-82.5	290	-72.5	155	-62.5	-85	-52.5	-290	-42.5	-229
-82	290	-72	110	-62	-28	-52	-298	-42	-278
-81.5	289	-71.5	65	-61.5	51	-51.5	-292	-41.5	-296
-81	289.4	-71	47	-61	120	-51	-266	-41	-297
-80.5	289.3	-70.5	-60	-60.5	75	-50.5	-225	-40.5	-275

Table C.1: Voltage at mixer output vs DOA measurements for $d = 7.5\lambda$ (-90 to -39.5 deg).

Angle	Volts	Angle	Volts	Angle	Volts	Angle	Volts
-40	-232	-30	-21	-20	288	-10	58
-39.5	-148	-29.5	110	-19.5	290	-9.5	-158
-39	-46	-29	215	-19	257	-9	-250
-38.5	95	-28.5	272	-18.5	191	-8.5	-289
-38	193	-28	289	-18	85	-8	-298
-37.5	258	-27.5	286	-17.5	-50	-7.5	-270
-37	287	-27	250	-17	-186	-7	-202
-36.5	292	-26.5	181	-16.5	-267	-6.5	-84
-36	270	-26	87	-16	-296	-6	75
-35.5	223	-25.5	-43	-15.5	-292	-5.5	200
-35	151	-25	-178	-15	-253	-5	271
-34.5	56	-24.5	-257	-14.5	-171	-4.5	293
-34	-81	-24	-289	-14	-33	-4	288
-33.5	-189	-23.5	-298	-13.5	108	-3.5	230
-33	-263	-23	-277	-13	226	-3	145
-32.5	-290	-22.5	-219	-12.5	277	-2.5	20
-32	-298	-22	-115	-12	294	-2	-135
-31.5	-277	-21.5	30	-11.5	272	-1.5	-244
-31	-228	-21	167	-11	217	-1	-287
-30.5	-145	-20.5	253	-10.5	121	-0.5	-297

Table C.2: Voltage at mixer output vs DOA measurements for $d = 7.5\lambda$ (-40 to 0.5 deg).

Angle	Volts	Angle	Volts	Angle	Volts	Angle	Volts
0	-297.8	10	249	20	262	30	-168
0.5	-209	10.5	289	20.5	50	30.5	-245
1	-94	11	289.5	21	-70	31	-283
1.5	60	11.5	259	21.5	-203	31.5	-298
2	192	12	186	22	-263	32	-288
2.5	260	12.5	85	22.5	-293	32.5	-257
3	293	13	-60	23	-296	33	-191
3.5	282	13.5	-188	23.5	-270	33.5	-82
4	236	14	-268	24	-210	34	39
4.5	147	14.5	-295	24.5	-121	34.5	159
5	34	15	-293	25	-18	35	231
5.5	-127	15.5	-263	25.5	142	35.5	278
6	-226	16	-187	26	228	36	293
6.5	-282	16.5	-66	26.5	274	36.5	285
7	-298	17	77	27	293	37	260
7.5	-280	17.5	200	27.5	284	37.5	200
8	-236	18	272	28	248	38	121
8.5	-123	18.5	293	28.5	182	38.5	30
9	38	19	283	29	76	39	-97
9.5	60	19.5	234	29.5	-30	39.5	-197

Table C.3: Voltage at mixer output vs DOA measurements for $d = 7.5\lambda$ (0 to 39.5 deg).

Angle	Volts	Angle	Volts	Angle	Volts	Angle	Volts	Angle	Volts
40	-257	50	1	60	291	70	-293	80	13.2
40.5	-285	50.5	-93	60.5	294	70.5	-285	80.5	42
41	-298	51	-179	61	290	71	-275	81	66
41.5	-293	51.5	-238	61.5	281	71.5	-264	81.5	92
42	-272	52	-270	62	266	72	-250	82	111
2.5	-235	52.5	-292	62.5	246	72.5	-236	82.5	133
43	-172	53	-298	63	217	73	-222	83	147
43.5	-85	53.5	-291	63.5	184	73.5	-207	83.5	156
44	9	54	-271	64	146	74	-194	84	161
44.5	108	54.5	-241	64.5	95	74.5	-182	84.5	162
45	186	55	-200	65	40	75	-170	85	162
45.5	238	55.5	-140	65.5	-27.8	75.5	-158	85.5	163.5
46	273	56	-65	66	-96	76	-147	86	167.7
46.5	290	56.5	5	66.5	-172	76.5	-134	86.5	175
47	292	57	87	67	-221	77	-118	87	188
47.5	282	57.5	151	67.5	-257	77.5	-101	87.5	192
48	253	58	203	68	-279	78	-80	88	219
84.5	211	58.5	239	68.5	-291	78.5	-57	88.5	233
49	156	59	266	69	-297	79	-35	89	240
49.5	83	59.5	282	69.5	-297.5	79.5	-10	89.5	251

Table C.4: Voltage at mixer output vs DOA measurements for $d = 7.5\lambda$ (40 to 89.5 deg).

Angle	Volts	Angle	Volts	Angle	Volts	Angle	Volts	Angle	Volts
-90	239	-80	230	-70	239	-60	-286	-50	140
-89.5	240	-79.5	237	-69.5	213	-59.5	-277	-49.5	84
-89	239	-79	243	-69	187	-59	-263	-49	6
-88.5	238	-78.5	248	-68.5	151	-58.5	-245	-48.5	-79
-88	233	-78	253	-68	118	-58	-215	-48	-153
-87.5	229	-77.5	259	-67.5	108	-85.5	-169	-47.5	-217
-87	222	-77	263	-67	67	-57	-108	-47	-254
-86.5	234	-76.5	266	-66.5	-39	-56.5	-14	-46.5	-275
-86	205	-76	269	-66	-90	-56	63	-46	-288
-85.5	200	-75.5	273	-65.5	-140	-55.5	144	-45.5	-294
-85	193	-75	275	-65	-184	-55	198	-45	-290
-84.5	190.8	-74.5	277	-64.5	-213	-54.5	244	-44.5	-280
-84	190.8	-74	279	-64	-238	-54	265	-44	-257
-83.5	192	-73.5	280	-63.5	-256	-53.5	277	-43.5	-222
-83	196	-73	279	-63	-269	-53	281	-43	-165
-82.5	199	-72.5	277	-62.5	-279	-52.5	277	-42.5	-71
-82	206	-72	274	-62	-287	-52	264	-42	36
-81.5	212	-71.5	267	-61.5	-292	-51.5	248	-41.5	137
-81	218	-71	260	-61	-293	-51	222	-41	200
-80.5	224	-70.5	247	-60.5	-291	-50.5	187	-40.5	249

Table C.5: Voltage at mixer output vs DOA measurements for $d = 6\lambda$ (-90 to -39.5deg).

Angle	Volts	Angle	Volts	Angle	Volts	Angle	Volts
-40	270	-30	122	-20	-55	-10	71
-39.5	281	-29.5	205	-19.5	134	-9.5	195
-39	280	-29	253	-19	216	-9	244
-38.5	266	-28.5	274	-18.5	262	-8.5	275
-38	241	-28	282	-18	279	-8	282
-37.5	206	-27.5	275	-17.5	281	-7.5	270
-37	147	-27	256	-17	265	-7	241
-36.5	70	-26.5	222	-16.5	233	-6.5	192
-36	-31	-26	174	-16	178	-6	104
-35.5	-125	-25.5	90	-15.5	102	-5.5	-3
-35	-211	-25	-5	-15	-15	-5	-132
-34.5	-257	-24.5	-123	-14.5	-142	-4.5	-220
-34	-282	-24	-213	-14	-232	-4	-272
-33.5	-293	-23.5	-265	-13.5	-273	-3.5	-292
-33	-291	-23	-288	-13	-292	-3	-292.8
-32.5	-276	-22.5	-294	-12.5	-292.8	-2.5	-275
-32	-250	-22	-285	-12	-277	-2	-245
-31.5	-202	-21.5	-260	-11.5	-240	-1.5	-172
-31	-109	-21	-214	-11	-179	-1	-50
-30.5	18	-20.5	-130	-10.5	-53	-0.5	96

Table C.6: Voltage at mixer output vs DOA measurements for $d = 6\lambda$ (-40 to 0.5 deg).

Angle	Volts	Angle	Volts	Angle	Volts	Angle	Volts
0	197	10	258	20	270	30	246
0.5	250	10.5	277	20.5	282	30.5	271
1	277	11	281	21	276	31	282
1.5	282	11.5	270	21.5	251	31.5	278
2	268	12	235	22	208	32	261
2.5	237	12.5	183	22.5	140	32.5	231
3	179	13	100	23	44	33	187
3.5	93	13.5	-15	23.5	-76	33.5	116
4	-15	14	-143	24	-179	34	31
4.5	-153	14.5	-230	24.5	-243	34.5	-76
5	-233	15	-270	25	-277	35	-167
5.5	-276	15.5	-291	25.5	-292	35.5	-239
6	-292	16	-293	26	-294	36	-270
6.5	-291	16.5	-277	26.5	-281	36.5	-289
7	-271	17	-247	27	-256	37	-295
7.5	-230	17.5	-181	27.5	-211	37.5	-286
8	-146	18	-65	28	-127	38	-267
8.5	10	18.5	73	28.5	-7	38.5	-235
9	124	19	177	29	115	39	-176
9.5	207	19.5	242	29.5	195	39.5	-91

Table C.7: : Voltage at mixer output vs DOA measurements for $d = 6\lambda$ (0 to 39.5 deg).

Angle	Volts	Angle	Volts	Angle	Volts	Angle	Volts	Angle	Volts
40	17	50	-294	60	260	70	-294.2	80	-140
40.5	111	50.5	-292	60.5	248	70.5	-292	80.5	-118
41	191	51	-284	61	231	71	-289	81	-100
41.5	238	51.5	-267	61.5	214	71.5	-285	81.5	-75
42	262	52	-242	62	194	72	-281	82	-52
2.5	277	52.5	-210	62.5	170	72.5	-277	82.5	-31
43	282	53	-160	63	145	73	-273	83	-9.9
43.5	278	53.5	-90	63.5	114	73.5	-268	83.5	5.7
44	266	54	-11.5	64	78	74	-263	84	17.7
44.5	246	54.5	56	64.5	34	74.5	-258	84.5	22.6
45	219	55	125	65	-9	75	-252	85	2.9
45.5	187	55.5	177	65.5	-68	75.5	-246	85.5	20.3
46	128	56	216	66	-125	76	-238	86	18.4
46.5	62	56.5	243	66.5	-185	76.5	-230	86.5	29
47	-19	57	264	67	-227	77	-220	87	59
47.5	-110	57.5	275	67.5	-255	77.5	-210	87.5	98
48	-188	58	281	68	-273	78	-200	88	126
84.5	-239	58.5	282	68.5	-285	78.5	-186	88.5	142
49	-266	59	278	69	-291	79	-172	89	148
49.5	-285	59.5	270	69.5	-294	79.5	-156	89.5	150

Table C.8: Voltage at mixer output vs DOA measurements for $d = 6\lambda$ (40 to 89.5 deg).

Angle	Volts	Angle	Volts	Angle	Volts	Angle	Volts	Angle	Volts
-90	111	-80	274	-70	-174	-60	245	-50	177
-89.5	104	-79.5	278.5	-69.5	-224	-59.5	211	-49.5	91
-89	89	-79	280.7	-69	-256	-59	157	-49	-48
-88.5	75	-78.5	281.2	-68.5	-278	-58.5	87	-48.5	-177
-88	65	-78	280.3	-68	-287	-58	-29	-48	-247
-87.5	63	-77.5	277.7	-67.5	-286	-85.5	-143	-47.5	-282
-87	70.9	-77	273.6	-67	-273	-57	-220	-47	-288
-86.5	85	-76.5	268.6	-66.5	-252	-56.5	-269	-46.5	-272
-86	105	-76	261	-66	-219	-56	-285	-46	-237
-85.5	127	-75.5	252.3	-65.5	-172	-55.5	-286	-45.5	-164
-85	149	-75	242.1	-65	-90	-55	-271	-45	-14
-84.5	170	-74.5	229	-64.5	14	-54.5	-230	-44.5	129
-84	187	-74	211	-64	105	-54	-168	-44	219
-83.5	205	-73.5	191	-63.5	168	-53.5	-15	-43.5	265
-83	219	-73	165	-63	217	-53	129	-43	280
-82.5	231	-72.5	129	-62.5	248	-52.5	218	-42.5	263
-82	244	-72	86	-62	268	-52	266	-42	214
-81.5	254	-71.5	28	-61.5	279	-51.5	280	-41.5	113
-81	263	-71	-27	-61	278.7	-51	269	-41	-12
-80.5	269	-70.5	-109	-60.5	268.2	-50.5	237	-40.5	-179

Table C.9: Voltage at mixer output vs DOA measurements for $d = 10\lambda$ (-90 to -39.5 deg).

Angle	Volts	Angle	Volts	Angle	Volts	Angle	Volts
-40	-258	-30	233	-20	-289	-10	7
-39.5	-289	-29.5	275	-19.5	-271	-9.5	-125
-39	-282	-29	273	-19	-211	-9	-244
-38.5	-241	-28.5	233	-18.5	-38	-8.5	-287
-38	-150	-28	142	-18	175	-8	-273
-37.5	38	-27.5	40	-17.5	256	-7.5	-212
-37	187	-27	-204	-17	281	-7	-30
-36.5	256	-26.5	-275	-16.5	252	-6.5	156
-36	280	-26	-289	-16	161	-6	258
-35.5	215	-25.5	-261	-15.5	5	-5.5	282
-35	115	-25	-197	-15	-200	-5	252
-34.5	60	-24.5	-15	-14.5	-274	-4.5	170
-34	-60	-24	160	-14	-285	-4	-29
-33.5	-199	-23.5	255	-13.5	-253	-3.5	-214
-33	-274	-23	280	-13	-144	-3	-278
-32.5	-288	-22.5	262	-12.5	85	-2.5	-280
-32	-266	-22	182	-12	213	-2	-230
-31.5	-211	-21.5	36	-11.5	276	-1.5	-101
-31	-47	-21	-157	-11	273	-1	120
-30.5	139	-20.5	-256	-10.5	210	-0.5	242

Table C.10: Voltage at mixer output vs DOA measurements for $d = 10\lambda$ (-40 to 0.5 deg).

Angle	Volts	Angle	Volts	Angle	Volts	Angle	Volts
0	280	10	-81	20	-274	30	261
0.5	266	10.5	135	20.5	-261	30.5	201
1	197	11	251	21	-177	31	91
1.5	53	11.5	281	21.5	-9	31.5	-107
2	-169	12	261	22	175	32	-234
2.5	-263	12.5	177	22.5	263	32.5	-280
3	-287	13	16	23	282	33	-284
3.5	-260	13.5	-172	23.5	254	33.5	-256
4	-182	14	-270	24	182	34	-188
4.5	31	14.5	-287	24.5	42	34.5	-54
5	193	15	-261	25	-137	35	140
5.5	270	15.5	-184	25.5	-247	35.5	227
6	281	16	19	26	-285	36	273
6.5	237	16.5	191	26.5	-278	36.5	281
7	140	17	264	27	-236	37	248
7.5	-57	17.5	281	27.5	-133	37.5	181
8	-224	18	240	28	65	38	68
8.5	-284	18.5	140	28.5	202	38.5	-95
9	-276	19	-13	29	263	39	-194
9.5	-228	19.5	-207	29.5	282	39.5	-272

Table C.11: : Voltage at mixer output vs DOA measurements for $d = 10\lambda$ (0 to 39.5 deg).

Angle	Volts	Angle	Volts	Angle	Volts	Angle	Volts	Angle	Volts
40	-287	50	52	60	-184	70	-215	80	-102
40.5	-240	50.5	166	60.5	-125	70.5	-243	80.5	-72
41	-166	51	235	61	-32	71	-261	81	-38
41.5	-6	51.5	268	61.5	66	71.5	-283	81.5	-3
42	141	52	282	62	141	72	-284	82	43
2.5	225	52.5	271	62.5	193	72.5	-285	82.5	83
43	267	53	243	63	235	73	-284	83	118
43.5	282	53.5	194	63.5	261	73.5	-282	83.5	145
44	270	54	147	64	276	74	-278	84	172
44.5	239	54.5	15	64.5	282	74.5	-272	84.5	202
45	176	55	-80	65	275	75	-266	85	215
45.5	82	55.5	-188	65.5	259	75.5	-258	85.5	225
46	-58	56	-243	66	232	76	-250	86	233
46.5	-171	56.5	-271	66.5	192	76.5	-241	86.5	239
47	-249	57	-284	67	142	77	-230	87	242.5
47.5	-286	57.5	-286	67.5	84	77.5	-212	87.5	242.5
48	-275	58	-279	68	20	78	-187	88	240.5
84.5	-247	58.5	-267	68.5	-56	78.5	-165	88.5	236
49	-192	59	-248	69	-122	79	-147	89	228
49.5	-111	59.5	-220	69.5	-178	79.5	-124	89.5	216

Table C.12: Voltage at mixer output vs DOA measurements for $d = 10\lambda$ (40 to 89.5 deg)

LIST OF REFERENCES

1. Herndon H. Jenkins, *Small-Aperture Radio Direction Finding*, Artech House Inc, Norwood, MA, 1991.

2. Byron Edde, *Radar Principles, Technology, Applications*, Prentice-Hall, Inc, Upper Saddle Ricer, NJ, 1993.

3. Matthew Sadiku, *Elements of Electromagnetics*, Saunders College Publishing, Orlando, FL, 1994.

4. Luis E. Moita Rodrigues, "High-Resolution Residue Antenna Architectures for Wideband Direction Finding," Naval Postgraduate School Master's Thesis, June 1996.

5. Byeong-Jun Park, "Interpolation Techniques in High-Resolution Residue Antenna Architectures," Naval Postgraduate School Master's Thesis, September 1996.

6. P. E. Pace, J. L. Schafer, D. Styer, "Optimum Analog Preprocessing for Folding ADCs," *IEEE Transactions on Circuits and Systems-II Analog and Digital Signal Processing,* Vol. 42, No 12, pp 825-829, December 1989.

INITIAL DISTRIBUTION LIST